Structural and functional analysis of pullulanase from *Klebsiella pneumoniae*

Naoki Saka

2019

Structural and functional analysis of pullulanase from *Klebsiella pneumoniae*

contents

List of Accession Number

The determined crystal structures in this thesis have been submitted to the RCSB Protein Data Bank (http://www.rcsb.org/pdb/) under the accession number as follows:

Klebsiella pneumoniae pullulanase of space group $P4_32_12$	5YN2
Klebsiella pneumoniae pullulanase/0.1 mM β-cyclodextrin	5YN7
Klebsiella pneumoniae pullulanase/1 mM α-cyclodextrin	5YNA
Klebsiella pneumoniae pullulanase/1 mM β-cyclodextrin	5YNC
Klebsiella pneumoniae pullulanase/1 mM γ-cyclodextrin	5YND
Klebsiella pneumoniae pullulanase/10 mM α-cyclodextrin	5YNE
Klebsiella pneumoniae pullulanase/10 mM γ-cyclodextrin	5YNH
PulA-G680 from *Klebsiella pneumoniae* / ligand-free	6J33
PulA-G680 from *Klebsiella pneumoniae* / maltotriose	6J34
PulA-L680 mutant from *Klebsiella pneumoniae* /ligand-free	6J35
PulA-L680 mutant from *Klebsiella pneumoniae* /maltotriose	6J4H

Introduction

Pullulanases (EC 3.2.1.41) hydrolyze α-1,6-glycosidic linkage of α-glucan such as amylopectin, glycogen and pullulan, a polymer consisted of maltotriose units linked by α-1,6-glycosidic linkage. These enzymes are found widely in bacteria, archaea and Eukaryota.

Pullulanases belong to glycoside hydrolase family 13 (GH13), known as α-amylase family, even among 42 subfamilies, belong to subfamily 12-14 in the Carbohydrate-Active enZymes (CAZy) database (Lombard et al., 2014). GH13 has $(\beta/\alpha)_8$-TIM barrel as a common structure and has four conserved regions in active site.

Pullulanase was first isolated from *Aerobacter aerogenes* (*Klebsiella pneumoniae*; Bender & Wallenfels, 1961). *Klebsiella pneumoniae* pullulanase (KPP) was reported three-dimensional structure by Mikami et al. (2006) and is consisted of CBM41, N2 domain, CBM48, A and C domain (Fig. 1).

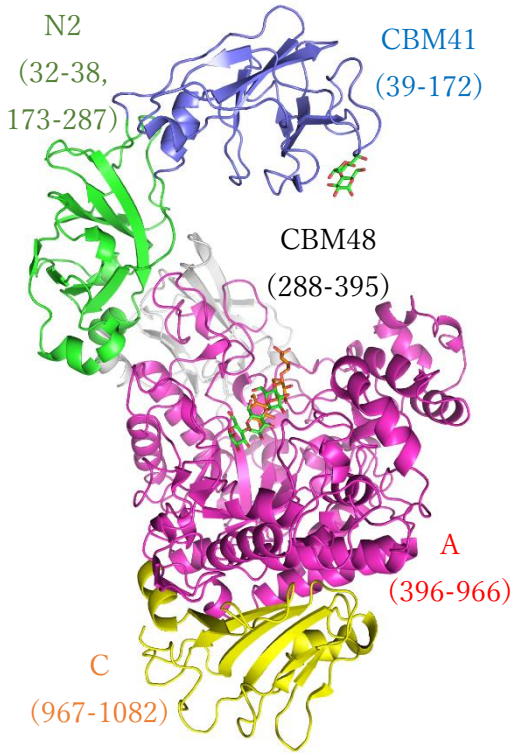

Figure 1. Overall structure of *Klebsiella pneumoniae* pullulanase (CBM41, purple; N2domain, green; CBM48, grey; A domain, magenta; C domain, yellow). Glucose molecules are shown as stick models.

Cyclodextrins (CD) are cyclo-oligosaccharides consisted of glucoses linked by α-1,4-glycosidic bond. Cyclo-oligosaccharides including six-, seven-, eight-glucoses named α-, β-, γ-CD, respectively (Fig. 2). Inside of CD ring is hydrophobicity, therefore, CDs form inclusion compounds for several hydrophobic compounds. CDs are known to inhibitors for α-amylases, pullulanases are also inhibited. Almost α-amylases are inhibited by CDs, especially α-CD is strong inhibitor. However, pullulanases are strongest inhibited by β-CD. Same such as other pullulanases, KPP is also strongest inhibited by β-CD. Inhibition constant of β-CD is 100 times much than that of α-CD and γ-CD (Iwamoto et al., 1993; Iwamoto et al., 1994).

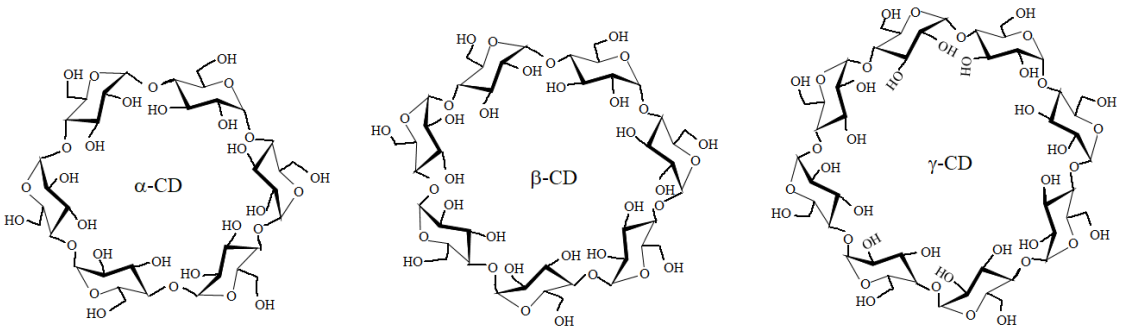

Figure 2. Chemical structures of α-, β-, γ-cyclodextrin.

KPP has characteristic structure in active site. Loop including residues 706-710 changes depending on substrate binding (Fig. 3). Other than KPP, many pullulanase structures such as *Streptococcus agalactiae* pullulanase (Gourlay et al., 2009), *Streptococcus pneumoniae* pullulanase (Lammert et al., 2011), *Klebsiella oxytoca* pullulanase (East et al., 2016), *Anoxybacillus* sp. LM 18-11 pullulanase (Xu et al., 2014), *Bacillus acidopullulyticus* pullulanase (Turkenburg et al., 2009), and *Bacillus substilis* str. 168 pullulanase (Malle et al., 2006) were solved. Common to these

structures, loop structures did not change depending on substrate binding, different from KPP.

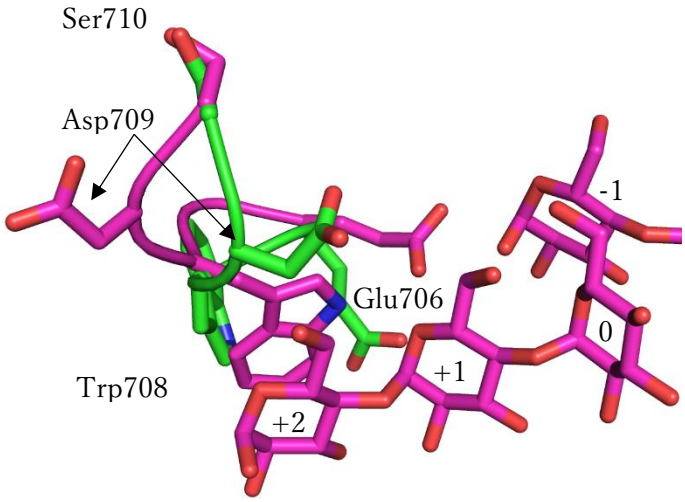

Figure 3. Conformational change of active site loop of *Klebsiella pneumoniae* pullulanase. The green and magenta sticks show ligand-free and maltotriose-complex structures, respectively.

This thesis reveals the biochemical property of *Klebsiella pneumoniae* pullulanase from crystal structure. Chapter 1 shows mechanism of interaction between *Klebsiella pneumoniae* pullulanase and cyclodextrins. Chapter 2 shows the cause of conformational change of loop in active site of *Klebsiella pneumoniae* pullulanase.

References

Bender, H. & Wallenfels, K. (1961). *Biochem. Z.* **334**, 79.

East, A., Mechaly, A E., Huysmans, G H., Bernarde, C., Tello-Manigne, D., Nadeau, N., Pugsley, A P., Buschiazzo, A., Alzari, P M., Bond, P J. & Francetic, O. (2016). *Structure*, **24**, 92-104.

Gourlay, L. J., Santi, I., Pezzicoli, A., Grandi, G., Soriani, M. & Bolognesi, M. (2009). J. Bacteriol. 191, 3544-3552.

Iwamoto, H., Ohmori, M., Ohno, M., Hirose, J., Hiromi, K., Fukada, H., Takahashi, K., Hashimoto, H. & Sakai, S. (1993). *J. Biochem.* **113**, 93-96.

Iwamoto, H., Ohno, M., Ohmori, M., Hirose, J., Tanaka, A., Sakai, S. & Hiromi, K. (1994). *J. Biochem.* **116**, 1264-1268.

Lammert van Bueren, A., Ficko-Blean, E., Pluvinage, B., Hehemann, J. H., Higgins, M. A., Deng, L., Ogunniyi, A. D., Stroeher, U. H., El, Warry, N., Burke, R. D., Czjzek, M., Paton, J. C., Vocadio, D. J. & Boraston, A. B. (2011). *Structure.* **19**, 640-651.

Lombard, V., Golaconda Ramulu, H., Drula, E., Coutinho, P. M. & Henrissat, B. (2014). *Nucleic Acids Res*. **42**, D490-D495.

Malle, D., Itoh, T., Hashimoto, W., Murata, K., Utsumi, S. & Mikami, B. (2006). *Acta Cryst. F* **62**, 381-384.

Mikami, B., Iwamoto, H., Malle, D., Yoon, H.-J., Demirkan-Sarikaya, E., Mezaki, Y. & Katsuya, Y. (2006). *J. Mol. Biol.* **359**, 690-707.

Turkenburg, J. P., Brzozowski, A. M., Svendsen, A., Borchert, T. V., Davies, G. J. & Wilson, K. S. (2009). *Protein*. **76**, 516-519.

Xu, J., Ren, F., Huang, C. H., Zheng, Y., Zhen, J., Sun, H., Ko, T P., He, M., Chen, C. C., Chan, H. C., Guo, R. T., Song, H. & Ma, Y. (2014). *Protein*. **82**, 1685-1693.

Chapter 1

Elucidation of the mechanism of interaction between *Klebsiella pneumoniae* pullulanase and cyclodextrin

1. Introduction

Starch-debranching enzymes hydrolyse α-1,6-glycosidic linkage of α-glucans such as amylopectin, glycogen and pullulan. These enzymes are divided into three types according to their substrate specificity. Isoamylases (EC 3.2.1.68) mainly hydrolyse amylopectin and glycogen, but not pullulan. Limit dextrinases (EC 3.2.1.142) mainly hydrolyse pullulan and amylopectin, but not glycogen. Pullulanases hydrolyse α-1,6-glycosidic linkage of pullulan, amylopectin and glycogen (Manners 1997). These enzymes and some α-amylases belong to the same α-amylase family, which is classified as glycoside hydrolase family 13 in the Carbohydrate-Active enZymes (CAZy) database (Lombard et al., 2014).

Pullulanase was first isolated from *Aerobacter aerogenes* (*Klebsiella pneumoniae*) (Bender & Wallenfels, 1961). We previously reported the three-dimensional structure of *Klebsiella pneumoniae* pullulanase (KPP) as the first resolved structure of a pullulanase (Mikami et al., 2006). The structure of KPP consists of five domains: CBM41 from residues 39-172, the N2 domain from 32-38 and 173-287, CBM48 from 288-395, the A domain from 396-966 (catalytic domain), and the C domain from 967-1083 (DUF3372). Since then, the three-dimensional structures of several pullulanases have been reported: *Streptococcus agalactiae* pullulanase (Gourlay et al., 2009), *Streptococcus pneumoniae*

pullulanase (Lammert et al., 2011), *Klebsiella oxytoca* pullulanase (East et al., 2016), *Anoxybacillus* sp. LM 18-11 pullulanase (Xu et al., 2014), *Bacillus acidopullulyticus* pullulanase (Turkenburg et al., 2009), and *Bacillus substilis* str. 168 pullulanase (Malle et al., 2006). Moreover, the structural information of other debranching enzymes, i.e., *Hordeum vulgare* limit dextrinase (*Hv*LD; Vester-Christensen et al., 2010B; Møller et al., 2015A; Møller et al., 2015B), *Bacillus stearothermophilus* neopullulanase (Hondoh et al., 2003), *Chlamydomonas reinhardtii* isoamylase I (Sim et al., 2014) and *Pseudomonas amyloderamosa* isoamylase (Katsuya et al., 1998) were stored at the RCSB Protein Data Bank (www.rcsb.org/).

Cyclodextrins (CDs) are cyclic oligosaccharides consisting of α-1,4-glycosidic-linked α-D-glucose units and are known to occur in three types: α-CD (six-glucose units), β-CD (seven-glucose units) and γ-CD (eight-glucose units) (Szejtli, 1998). CD, especially α-CD, imitates the helix structure of amylose and is a strong inhibitor of some starch active enzymes, including α- and β-amylases (Marshall, 1973). Interestingly, it has been reported that the interaction between KPP and β-CD is different from those between KPP and α-/γ-CD. The dissociation constant (*Kd*) and inhibition constant (*Ki*) of β-CD are more than 100 times smaller than those of α-/γ-CDs (Iwamoto et al., 1993; Iwamoto et al., 1994).

In this paper, we reported the three-dimensional structures of the KPP/α-, β-, γ-CD complexes. These structures revealed that two CDs bind to the edge of CBM41 and the active site of the A domain. We could explain the strong inhibition of β-CD based on the complex structure and the site-directed mutation. It is concluded that the interactions between the active site of KPP and CDs depend on the kinds and the concentration of

CDs mainly caused by the hydrophobic interaction of inner ring cavity and the side chain of Phe746.

2. Experimental Procedures

2.1 Purification of the KPP

Crystallized KPP (Abdullah & French, 1970; Harada et al., 1972; Yokobayashi et al., 1973) was supplied by Hayashibara Co. (Okayama, Japan). The crystals were collected by centrifugation (10,000 rpm, 10 min, 277 K), and resuspended in 50 mM of sodium acetate buffer (pH 6.0). In order to remove ammonium sulfate, the protein solution was applied to a HiPrep^{TM} 26/10 Desalting column (GE Healthcare) previously equilibrated with 50 mM sodium acetate buffer (pH 6.0). The eluted protein solution was concentrated by Vivaspin6 (Sartorius Stedim Biotech GmbH) to a final concentration of 10 mg/mL.

2.2 Crystallization and X-ray diffraction

The protein solution consists of 9 mg/mL protein, and 50 mM sodium acetate buffer (pH 6.0) in the presence and absence of 0.1-10 mM CD. The initial screening for KPP crystallization was performed using the Crystal Screen I/II and PEG/Ion crystallization screening kits from Hampton Research (Aliso Viejo, CA) by the sitting-drop vapor diffusion method in a 96-well plate. The crystallization was started by mixing 1 μl of the protein solution with 1 μl of the reservoir solution (100 μl). In a few days, the crystals were grown under the condition of 0.01 M cobalt (II) chloride hexahydrate, 0.1 M 2-(*N*-morpholino) ethanesulfonic acid (MES) buffer (pH 6.5) and 1.8 M ammonium sulfate (Crystal Screen II No. 25) at 293 K. As these crystals gave low-resolution diffraction data (> 3.5 Å), a second screening was performed under protein solution containing 0.1 M

magnesium sulfate. Crystal clusters were gained under the condition of 0.2 M magnesium acetate and 20% (w/v) polyethylene glycol 3350 (PEG/Ion No. 25) at 293 K for one day. Single crystals were obtained by the micro-seeding method under the same conditions. Prior to flash-cooling, the crystals were briefly transferred into a cryo-protectant solution containing 10 – 30% (v/v) ethylene glycol or 20 – 30% (v/v) glycerol in mother solution. Diffraction data were collected using synchrotron radiation on beamlines BL26B1 and BL38B1 in SPring-8 (Hyogo, Japan) after a diffraction check using an in-house detector of a Bruker Hi-Star multiwire area detector coupled with Cu Kα radiation generated by a MAC Science M18XHF rotating anode. The collected diffraction data were processed with the program HKL2000 (Otwinowski & Minor, 1997).

2.3 Structure determination and refinement

The crystal structures of the ligand-free KPP and 6 KPP/CD complexes prepared in the presence of 0.1 mM β-CD, 1 mM α-, β-, and γ-CD and 10 mM α- and γ-CD were determined by the molecular replacement method using the atomic coordinates of KPP (PDB accession code: 2FHF) as a search model with MOLREP (Vagin & Teplyakov, 1997) from the CCP4 program suite (Collaborative Computational Project, Number 4, 1994). The structures were refined with REFMAC5 (Murshudov et al., 2011; Murshudov et al., 1997) from the CCP4 program suite and phenix.refine from the PHENIX program suite (Adams et al., 2002) at a resolution of 1.96 - 2.59 Å after model rebuilding with the program COOT (Emsley & Cowtan, 2004) as shown in Table.1. Ribbon and stick models were prepared using PyMOL (DeLano, 2002).

2.4 Definition of screw-axis

Superposition of structures was carried out using the programs FIT (Guoguang Lu, Lund University) and Profit (SciTech Software). CBM41 and the static cores of the N2,

CBM48, A and C domain were identified by a sieve-fit procedure (Lesk, 1991). Only Cα atoms were used for the fitting procedure and a 0.44 Å threshold was adopted. The screw-axis, rotation angle and translation distance were calculated from a matrix superimposing CBM41 of different crystals.

2.5 Cloning, expression and purification of recombinant *Klebsiella pneumoniae* pullulanase

The *Klebsiella pneumoniae* strain ATCC9621 (*Klebsiella pneumoniae* NBRC3321) was supplied by the Biological Resource Center, National Institute of Technology and Evaluation. The product pullulanase (PulA) from *Klebsiella pneumoniae* strain ATCC9621 is slightly different from KPP. There are mutations of two amino acid residues; one is Asn229 of KPP to Ser, another is Leu680 of KPP to Gly. A *PulA* gene of 3159 bp (32-1083 residues) coding for pullulanase from *Klebsiella pneumoniae* ATCC9621 was amplified by PCR using two primers, a forward primer (5'-GGAATTCCATATGGATGTCGTCGTCCGCTTACCG-3') including the *Nde*I restricted site (underlined) and a reverse primer (5'-GCTCTAGATTAGCCAAAGGCGGCGCGG-AAGGC-3') including the *Xba*I restricted site (underlined), and Hot Star Taq^{TM} DNA polymerase (QIAGEN). The amplified *PulA* gene was introduced into plasmid pCold^{TM} TF DNA (Takara Bio Co.) as a cloning vector using *Nde*I and *Xba*I and expressed as an N-terminal Trigger Factor including the His-tagged fusion protein in *Escherichia Coli* BL21. *E. Coli* BL21 was inoculated in a 5 L flask containing 1 L of LB medium supplemented with 50 μg/mL ampicillin and incubated at 37°C for 3 h. Protein expression was induced by 0.2 mM isopropyl-β-thiogalactopyranoside (IPTG) at 15°C for 20 h after incubating in ice water for 30 min when the absorbance at 600 nm reached

0.6. *E. Coli* cells were harvested by centrifugation at 6000 rpm for 10 min at 4°C. The paste was resuspended in 500 mM sodium chloride, 0.1 mM EDTA and 0.1% Triton-100 containing 20 mM Tris-HCl buffer (pH 7.3). After sonication, the lysate solution was centrifuged at 10,000 rpm for 10 min at 4°C and filtered through a 45 μm pore-size membrane. After the protein solution was loaded onto a column of Ni-NTA, the column was washed with 50 mM Tris-HCl buffer (pH 7.3) containing 20 mM imidazole and 300 mM sodium chloride. Proteins were eluted with a linear gradient of imidazole from 20 to 400 mM. Collected samples were dialyzed against 20 mM Tris-HCl (pH 7.3).

The F746A variant was prepared using primers containing the nucleotide substitution (forward:5'-GCCGGCC**GAC**TCCGGTGAC-3'; reverse:5'-GTCACCGGAGTC**GGC**-CGGC-3') and Ex Taq DNA Polymerase (Takara Bio Co.). The expression and purification of the F746A variant were performed as described above.

2.6 Activity and inhibition studies

PulA and PulA-F746A activities and inhibition constants were determined using the modified Park-Johnson method (Iwamoto et al. (1993), Iwamoto et al. (1994)). The Michaelis constant (K_m) and rate of a reaction (k_{cat}) were measured for the reaction mixture containing the substrate pullulan (0.00005-0.001%), PulA (5.0×10^{-10} M) or PulA-F746A (1.0×10^{-9} M), and 0.05 M sodium acetate buffer (pH 5.6) at 25°C. Inhibition constants of PulA were measured for the reaction mixture containing the substrate pullulan (0.00025-0.003%), PulA (5.0×10^{-10} M), inhibitors (0 and 30 μM for α-CD, 0 and 0.5 μM for β-CD, 0 and 20 μM for γ-CD) and 0.05 M sodium acetate buffer (pH 5.6) at 25°C. Inhibition constants of PulA-F746A were measured for the reaction mixture containing the substrate pullulan (0.00025-0.003%), PulA-F746A

(1.0×10^{-9} M), inhibitors (0 and 500 μM for α-CD, 0 and 500 μM for β-CD, 0 and 500 μM for γ-CD) and 0.05 M sodium acetate buffer (pH 5.6) at 25°C.

Table 1. Data collection and Refinement statistics

substrate analog (mM)	Ligand-free	β-CD (0.1)	α-CD (1)	β-CD (1)	γ-CD (1)	α-CD (10)	γ-CD (10)
A. Diffraction data							
X-ray source	SPring-8 BL38B1	SPring-8 BL26B1	SPring-8 BL26B1	SPring-8 BL26B1	SPring-8 BL26B1	SPring-8 BL26B1	SPring-8 BL26B1
Detector	mx225HE	mx225HE	mx225HE	mx225HE	mx225HE	mx225HE	mx225HE
Wavelength (Å)	1.00	1.00	1.00	1.00	1.00	1.00	1.00
Resolution range (Å)	39.3 - 2.30 (2.38 - 2.30)	44.16 - 2.59 (2.68 - 2.59)	44.15 - 1.96 (2.03 - 1.96)	43.98 - 2.32 (2.40 - 2.32)	43.39 - 2.23 (2.31 - 2.23)	49.75 - 2.20 (2.28 - 2.20)	49.67 - 2.05 (2.12 - 2.05)
Space group	$P4_32_12$	$P4_32_12$	$P4_32_12$	$P4_32_12$	$P4_32_12$	$P4_32_12$	$P4_32_12$
Unit cell parameters							
a (Å)	89.04	89.28	89.28	88.93	88.77	89.21	89.21
b (Å)	89.04	89.28	89.28	88.93	88.77	89.21	89.21
c (Å)	301.84	301.71	299.38	299.53	298.38	299.65	299.98
Unique reflections	54725 (5298)	38988 (3763)	87861 (8666)	53051 (5167)	59330 (5762)	62633 (6157)	76149 (7539)
Multiplicity	5.0 (5.1)	6.1 (6.3)	8.3 (8.2)	7.0 (7.1)	5.7 (5.8)	10.7 (10.5)	7.1 (7.2)
Completeness (%)	99.27 (98.22)	98.88 (97.71)	99.87 (99.94)	99.67 (98.70)	99.53 (99.21)	99.91 (99.64)	99.03 (99.31)
Mean $I/\sigma(I)$	18.08 (4.75)	16.22 (3.93)	22.35 (4.34)	18.35 (4.90)	16.86 (3.77)	28.44 (8.45)	19.04 (4.70)
Wilson *B*-factor (Å^2)	40.79	44.18	32.18	33.41	34.49	26.25	27.38
R_{merge} (%)	7.09 (53.7)	10.74 (45.64)	7.55 (47.45)	8.68 (48.47)	8.40 (51.35)	10.01 (41.57)	9.92 (42.79)
R_{meas} (%)	7.93 (59.7)	11.76 (49.8)	8.04 (47.5)	9.38 (52.2)	9.27 (56.5)	10.5 (43.7)	10.7 (46.1)
R_{pim} (%)	3.49 (25.9)	4.68 (19.5)	2.68 (17.3)	3.51 (19.3)	3.86 (23.3)	3.20 (13.3)	3.89 (16.8)
$CC_{1/2}$ (%)	99.8 (86.7)	99.6 (94.9)	99.8 (93.0)	99.8 (93.4)	99.8 (94.5)	99.8 (97.2)	99.7 (93.6)
B. Refinement statistics							
Reflections used in refinement	54658 (5298)	38868 (3753)	87819 (8662)	53040 (5166)	59280 (5748)	62621 (6156)	76130 (7533)
R_{work} (%)	18.45 (23.25)	19.10 (25.91)	19.82 (25.33)	18.72 (25.12)	19.07 (24.73)	18.13 (22.43)	20.57 (27.34)
R_{free} (%)	24.23 (28.59)	25.32 (36.30)	24.01 (29.97)	25.39 (31.76)	24.18 (32.89)	24.19 (32.17)	25.77 (34.83)
Number of							
Ca^{2+}/Mg^{2+}/Glc/Gol /EG/PEG/Ace	4/1/0/0 /0/0/0	5/0/7/0 /1/0/0	5/0/6/2 /0/1/2	5/0/14/1 /0/0/2	5/0/4/5 /0/2/0	5/0/12/6 /0/1/0	5/0/16/1 /0/0/0
water	416	208	496	382	290	544	349
Protein residues	1054	1054	1055	1052	1055	1054	1055
R.m.s.d., bond lengths (Å)	0.008	0.008	0.007	0.008	0.008	0.008	0.007
R.m.s.d., bond angles (deg.)	0.88	1.01	0.87	0.97	0.90	0.93	0.90
Ramachandran favored (%)	97.43	95.44	96.87	96.10	95.73	96.86	96.77
Rotamer outliers (%)	0.19	1.03	1.02	1.26	1.13	1.14	0.92
Clashscore	3.21	9.97	3.82	6.27	6.24	4.27	3.57
Average *B*-factor (Å^2)							
CBM41	65.6	69.1	54.1	52.3	55.4	41.9	44.9
N2 domain	55.7	55.0	51.5	56.6	61.7	42.4	49.4
CBM48	40.8	41.2	32.2	30.9	34.7	22.7	26.3
A domain	40.7	41.0	34.0	32.3	37.6	24.3	28.2
C domain	46.7	47.0	39.8	38.7	43.2	29.8	34.2
ligands	48.4	67.2	70.1	64.6	64.9	53.2	63.5
solvent	43.6	39.3	38.0	33.9	38.4	29.1	29.7
PDB ID	5YN2	5YN7	5YNA	5YNC	5YND	5YNE	5YNH

Statistics for the highest-resolution shell are shown in parentheses.

3. Results and discussion

3.1 Overall structure of the KPP ligand-free and CD complex

The crystals of the previously reported KPP (ligand-free and substrate-analog complexes) belonged to a space group of *C*2. From the protein packing of this *C*2 crystal, it was estimated that CBM41 of the symmetric molecule prevented the binding of large substrates such as CD to the active site (Mikami et al., 2006). In this study, we determined new crystallization conditions that yielded a space group of $P4_32_12$ for the ligand-free and CD complexes. In this space group, a symmetric molecule does not exist near the active site, which enabled the formation of KPP/CD complexes.

The values of r.m.s.d. of Cα atoms between the ligand-free and CD complexes was at most 0.7 Å. Because the relatively high r.m.s.d values were attributed to the difference in the position of CBM41 in each structure, we conclude that all the structures were nearly identical. In comparison with the reported G4 structure (PDB code 2FHF; Fig. 1*a*), CBM41, which was determined in the ligand-free structure of the present study, was rotated approximately 66°, and the value was 0.47 Å against superposition of the other domains (Fig. 1*b*). In the case of previous *C*2 crystals, CBM41 was visible only in the complexes with G3 and G4 because the *B*-factor of CBM41 was highest in ligand-free and complexes with G1 and isoG2 (Mikami et al., 2006). In the present space group of $P4_32_12$, CBM41s in all structures, even in the ligand-free form, were clearly visible because of the lower average *B*-factor (Table.1). In this crystal packing, CBM41 was stabilized by two symmetric molecules; one was on the surface opposite the active site of the A domain, and the other was on the C domain (Table.2).

3.2 The sugar conformation of bound CDs

KPP has two polysaccharide-binding sites: the tip of CBM41 and the active site (Fig. 2*a*). Among the 6 structures of CD complexes, two complexes, α-CD and γ-CD, do not contain CDs at the active site when they are present at lower concentration (1 mM). All glucose molecules in the bound CDs are in the $^4C_1$ pyranoside forms (Fig. 2*b*, *c* and Table.3), according to the Cremer-Pople parameter calculations (Cremer and Pople, 1975). The torsion angles were Φ = 101~135° and ψ = -130~-98° (Table.3), which are in the low-energy region of the isoenergy map (Imberty et al., 1988).

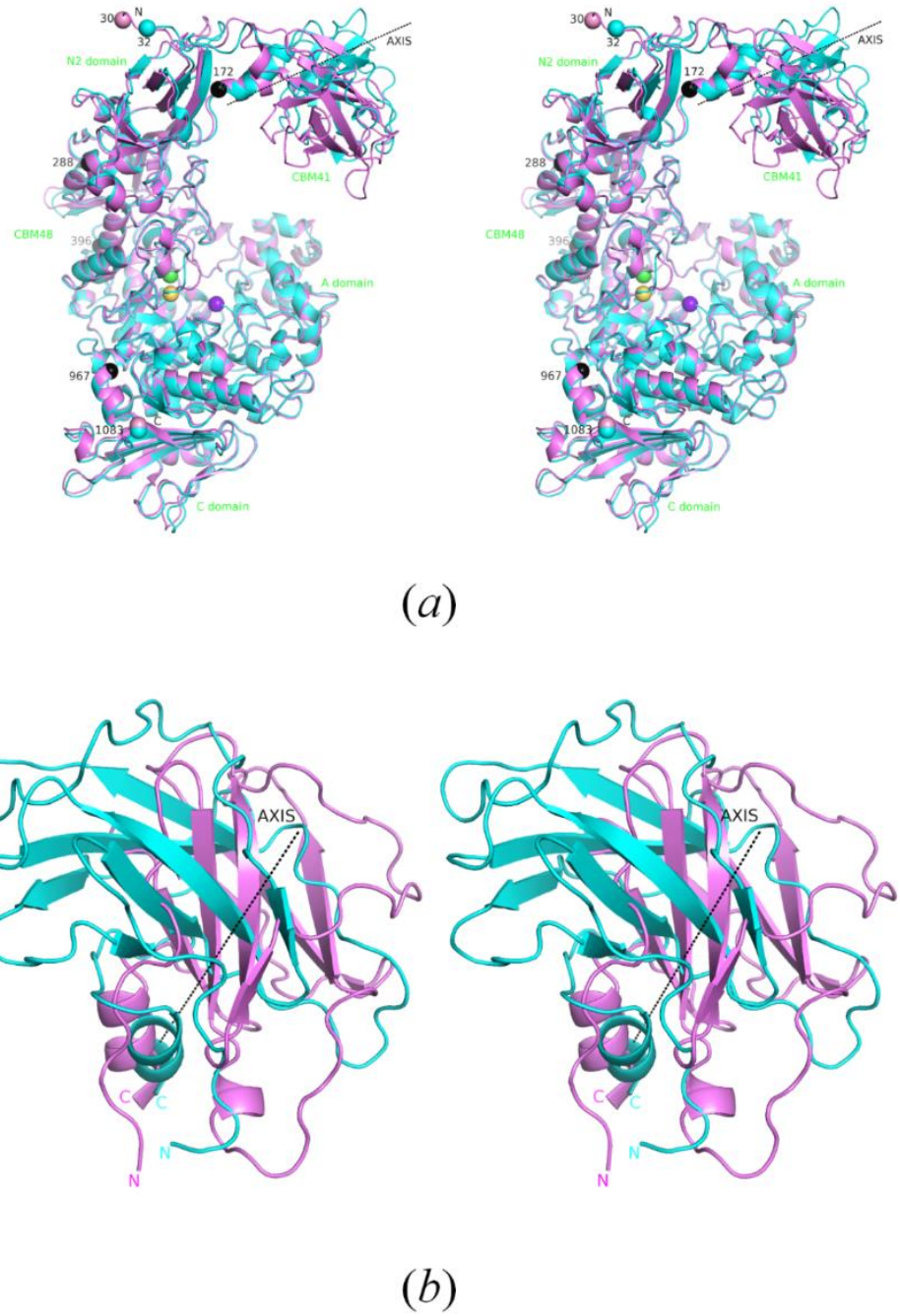

Figure 1
(*a*) Stereo representation of the overall structure comparison between ligand-free KPP ($P4_32_12$, pink) and KPP/G4 (C2: PDB code 2FHF, cyan). The apparent rotation axis is shown as a black dashed line. The pink spheres are N and C terminal residues of ligand-free KPP. The cyan spheres are N and C terminal residues of KPP/G4. The black spheres show the residues labelled in numbers. The green, yellow and purple spheres are Asp677 as nucleophile, Glu706 as acid/base and Asp834 as transition-state stabilizer, respectively. (*b*) Stereo representation of an enlarged view of CBM41 of ligand-free KPP (pink) superimposed on the overall structure of the KPP/G4 complex (cyan). The apparent rotation axis is shown as a black dashed line.

Table 2. Interaction between residues of CBM41 and symmetric molecules. Hydrogen bond (*a*) and C-C contact (*b*) distances were in the ranges of 2.45 Å to 3.24 Å and 3.95 Å to 4.44 Å, respectively. Distances were calculated using Contact from the CCP4 program suite (Collaborative Computational Project, Number 4, 1994). The apostrophe indicates a residue in the symmetric molecule.

(*a*)

		Hydrogen bond (Å)				
CBM41	Symmetry	1 mM α-CD	1 mM β-CD	1 mM γ-CD	10 mM α-CD	10 mM γ-CD
Glu45 N	Ser1082' O	2.86	2.87	2.84	2.82	2.65
Ala46 O	Ser1081' OG	2.89	3.07	3.00		2.95
Ser50 OG	Gly1077' O	2.77	3.12		2.73	2.61
Gln53 NE2	Asp1024' O	3.02	3.11		3.06	3.18
Ser105 OG	Asp982' OD2	3.02	3.20			
Lys107 N	Gly802' O	3.18	3.12	3.15	3.16	3.20
Glu45 O	Ser1081' OG		2.81	2.94		
Gln53 NE2	Ala1026' O		3.02	2.80		2.92
Thr68 OG1	Gln1037' OE1					3.19

(*b*)

	C-C contacts				
	Symmetry molecules				
CBM41	1 mM α-CD	1 mM β-CD	1 mM γ-CD	10 mM α-CD	10 mM γ-CD
Gly44	Lys1083'		Lys1083'	Lys1083'	Ser1083'
Gly44	Ser1082'	Ser1082'		Ser1082'	Ser1082'
Glu45	Ser1081'	Ser1081'	Ser1081'	Ser1081'	Ser1081'
Ala46		Ser1081'	Ser1081'	Ser1081'	
Val47	Ser1081'	Ser1081'		Ser1081'	Ser1081'
Val47	Arg977'	Arg977'	Arg977'	Arg977'	Arg977'
Gln48	Pro1079'	Pro1079'	Pro1079'	Pro1079'	Pro1079'
Gln48	Ser1081'	Ser1081'		Ser1081'	Ser1081'
Ser50			Pro1079'		Thr1028'
Arg52		Gly1027'	Gly1027'	Gly1027'	Gly1027'
Gln53		Thr1028'			Thr1028'
Thr68	Gln1037'	Gln1037'	Gln1037'		Gln1037'
Thr103	Gln1023'	Gln1023'	Gln1023'	Gln1023'	
Thr103	Asp1024'	Asp1024'	Asp1024'	Asp1024'	Asp1024'
Asp106	Gly802'	Gly802'	Gly802'	Gly802'	Gly802'
Asp106	Ile798'	Ile798'	Ile798'	Ile798'	Ile798'
Lys107	Gly802'	Gly802'	Gly802'	Gly802'	Gly802'
Lys107	Ala803'				Ala803'
Val113	Asp1024'	Asp1024'	Asp1024'	Asp1024'	Ala1024'
Pro115		Gly1027'	Gly1027'		
Pro115	Ala1026'	Ala1026'	Ala1026'	Ala1026'	Ala1026'
Asn132		Ala468'	Ala468'	Ala468'	Ala468'

Table 3. Sugar puckering parameters and torsion angles. The Tables of Cremer-Pople parameters and torsion angles for CDs bound to CBM41 (*a*) and the active site (*b*). Cremer-Pople parameters were calculated using a Web-site calculator (http://enzyme13.bt.a.u-tokyo.ac.jp/CP/). The torsion angles were calculated using the COOT program (Emsley and Cowtan, 2004). Torsion angles were defined as O5 – C1 – O4' – C4' (Φ) and C1 – O4' – C4' – C5' (ψ) between Glc 1 (include C1 atom) and Glc 2 (include O4 atom; dash number). (*a*)

		GLC 1	GLC 2	GLC 3	GLC 4	GLC 5	GLC 6	GLC 7	GLC 8
	Φ, θ (°)	111, 6	58, 17	357, 28	75, 16	118, 33	72, 23		
1 mM	Q	0.56	0.56	0.57	0.48	0.55	0.53		
α-CD	conformation	$^4C_1$	$^4C_1$	$^4C_1$	$^4C_1$	$^4C_1$	$^4C_1$		
	Φ, Ψ (°)	111, -130	105, -108	117, -123	108, -98	109, -108	109, -86		
	Φ, θ (°)	50, 13	358, 9	103, 17	344, 18	337, 5	26, 10	39, 14	
1 mM	Q	0.56	0.55	0.60	0.55	0.57	0.53	0.53	
β-CD	conformation	$^4C_1$	$^4C_1$	$^4C_1$	$^4C_1$	$^4C_1$	$^4C_1$	$^4C_1$	
	Φ, Ψ (°)	114, -130	129, -102	104, -117	109, -120	120, -112	118, -127	104, -116	
	Φ, θ (°)	21, 7	258, 10					28, 21	119, 16
1 mM	Q	0.57	0.58					0.63	0.52
γ-CD	conformation	$^4C_1$	$^4C_1$					$^4C_1$	$^4C_1$
	Φ, Ψ (°)	101, -117						107, -91	129, -116
	Φ, θ (°)	109, 7	66, 15	19, 17	77, 14	119, 38	67, 26		
10 mM	Q	0.54	0.55	0.53	0.54	0.51	0.50		
α-CD	conformation	$^4C_1$	$^4C_1$	$^4C_1$	$^4C_1$	$^4C_1$	$^4C_1$		
	Φ, Ψ (°)	110, -130	106, -98	110, -122	106, -101	114, -115	112, -86		
	Φ, θ (°)	21, 8	61, 7	92, 15	336, 21	116, 13	103, 6	338, 10	126, 33
10 mM	Q	0.55	0.53	0.54	0.52	0.56	0.54	0.56	0.51
γ-CD	conformation	$^4C_1$	$^4C_1$	$^4C_1$	$^4C_1$	$^4C_1$	$^4C_1$	$^4C_1$	$^4C_1$
	Φ, Ψ (°)	101, -128	135, -101	110, -133	129, -128	122, -119	126, -101	113, -123	120, -108

(*b*)

		GLC 1	GLC 2	GLC 3	GLC 4	GLC 5	GLC 6	GLC 7	GLC 8
	Φ, θ (°)	30, 10	34, 11	97, 17	17, 10	33, 10	72, 8	342, 13	
1 mM	Q	0.57	0.55	0.56	0.58	0.54	0.47	0.57	
β-CD	conformation	$^4C_1$	$^4C_1$	$^4C_1$	$^4C_1$	$^4C_1$	$^4C_1$	$^4C_1$	
	Φ, Ψ (°)	106, -129	118, -103	121, -105	114, -121	108, -118	118, -109	124, -119	
	Φ, θ (°)	28, 15	14, 17	29, 19	101, 11	47, 17	44, 10		
10 mM	Q	0.55	0.53	0.60	0.51	0.57	0.53		
α-CD	conformation	$^4C_1$	$^4C_1$	$^4C_1$	$^4C_1$	$^4C_1$	$^4C_1$		
	Φ, Ψ (°)	140, -131	107, -104	117, -120	110, -110	89, -99	117, -106		
	Φ, θ (°)	56, 12	82, 16	160, 7	77, 15	47, 10	58, 9	111, 27	305, 10
10 mM	Q	0.58	0.52	0.59	0.58	0.54	0.53	0.50	0.57
γ-CD	conformation	$^4C_1$	$^4C_1$	$^4C_1$	$^4C_1$	$^4C_1$	$^4C_1$	$^4C_1$	$^4C_1$
	Φ, Ψ (°)	104, -137	128, -102	123, -112	130, -112	93, -124	124, -105	123, -108	117, -121

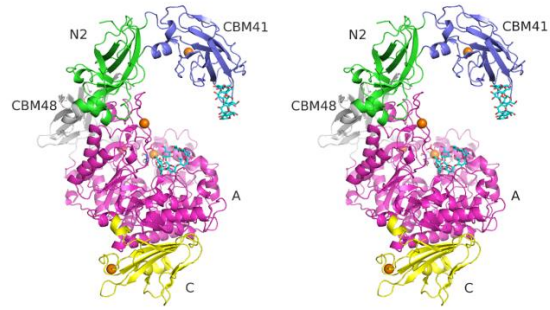

(*a*)

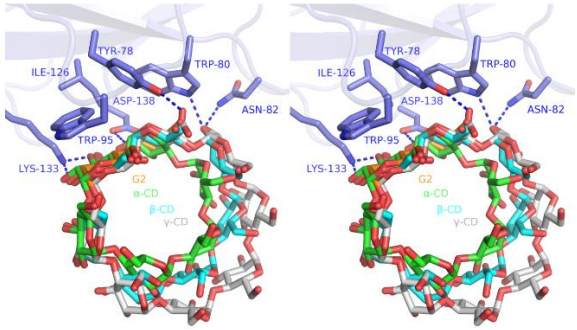

(*b*)

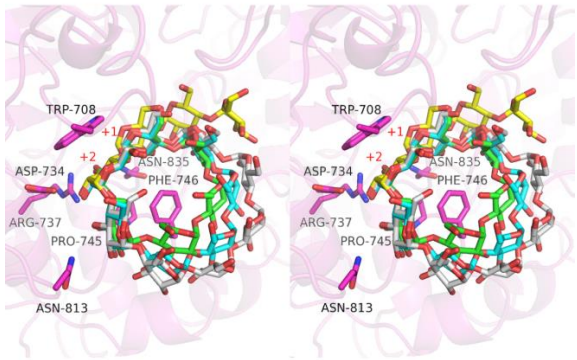

(*c*)

Figure 2 (*a*) Stereo representation of the overall structure of the KPP/β-CD complex at 1 mM (CBM41, purple; N2 domain, green; CBM48, grey; A domain, magenta; C domain, yellow). The orange spheres are calcium ions. The cyan, red and blue stick models are β-cyclodextrin, acetate ion and glycerol, respectively. (*b*) Stereo representation of the carbohydrate-binding site of CBM41. The purple, orange, green, cyan and grey sticks are binding residues, maltose of the part of maltotetraose in the KPP/G4 complex structure (PDB code 2FHF), α-cyclodextrin, β-cyclodextrin and γ-cyclodextrin, respectively. The blue dashed lines are hydrogen bonds. (*c*) Stereo representation of the interaction mode in the active site. The magenta, yellow, green, cyan and grey sticks are the binding residues maltotetraose in the KPP/G4 complex structure (PDB code 2FHF), α-cyclodextrin, β-cyclodextrin and γ-cyclodextrin, respectively.

3.3 The interaction between CBM41 and CDs

CBM41 of KPP was previously shown to bind with maltose (PDB code 2FHC and 2FHF) (Mikami et al., 2006). Recent studies have also shown that this CBM41 has strepadhesin activity for bacterial infection (Hytönen et al., 2003; Bueren et al., 2007). In this paper, we revealed that the interaction between CBM41 of KPP and CDs depends on the concentration of CDs used for the crystallization. In the complex with β-CD at 0.1 mM, there is no electron density of bound sugar in CBM41, whereas in the complex with 1 mM CDs, the α and β-CDs are clearly visible (Fig.3). In the case of the complex structure with 1 mM γ-CD, only the maltotetraose moiety is visible, while other parts are not clear (Fig.3*c*). In the complex structure with 10 mM γ-CD, the density map of γ-CD is observed (Fig.3*e*). Glc1 and Glc2 of α-CD and Glc1, Glc2 and Glc3 of β- and γ-CDs make 6-7 hydrogen bonds with 5 amino acid side-chains (Tyr78, Trp80, Asn82, Lys133 and Asp138) and many C-C contacts with protein residues (Trp80, Trp95, Ile126, Lys133 and Asp138), as shown in Table.4. Moreover, CDs bound with CBM41 were stabilized by interactions with the A domain of the symmetry molecules (Table.4). In the complex with α-CD, Glc6 makes a hydrogen bond with Asp594' and C-C contacts with Asp594' and Gln593' (the apostrophe indicates a residue in the symmetric molecule). In the complex with β-CD, Glc6 and Glc7 make 4 hydrogen bonds with Gln455', Gln593' and Asp594' and C-C contacts with Gln593' and Asp594'. In the complex with γ-CD, Glc7 and Glc8 make 3 hydrogen bonds with Wat215, Gln455' and Asp594' and C-C contacts with Gln593' and Asp594'.

3.4 The interaction between the active site and CDs

In most amylase/CD complex structures, hydrophobic side-chains such as Leu, Val, Phe and Tyr are thrust into the ring of CDs (Adachi et al., 1998; Larson et al., 2010; Mikami et al., 1993; Rejzek et al., 2011; Schmidt et al., 1998; Uitdehaag et al., 1999; Vester-Christensen et al., 2010B; Yokota et al., 2001). As shown in Fig. 2*c*, three CDs occupied subsites +2 and +1, whose subsites numbers were deduced from the complex with maltooligosaccharides (PDB code 2FHF; Mikami et al., 2006). Glc1 and Glc2 of α-, β- and γ-CD bind near the subsites +2 and +1 within r.m.s.d. of 2 Å, respectively. CDs interact with the side chains of 6 residues (Asp734, Arg737, Tyr812, Asn813, Asn835 and Arg889) by hydrogen bonds, and with the side chains of 8 residues (Trp708, Asp734, Arg737, Pro745, Phe746, Tyr812, Asn813 and Arg889) by C-C contacts (Table.5). The side chain of Phe746 interacts with the inner cavity of the ring of CDs in the same way as mentioned for the structures above (Fig. 4 and Fig. 5). The binding of CDs was dependent on the concentration of each CD in the active site. Only at a concentration of 10 mM, the α- and γ-CDs can bind to the active site (Fig. 4 *c* and *d*). On the other hand, β-CD interacts with the active site even at a concentration of 0.1 mM (Fig. 4 *a* and *b*). These results are in agreement with previous reports about the K_i values of the CDs (Iwamoto et al., 1993; Iwamoto et al., 1994).

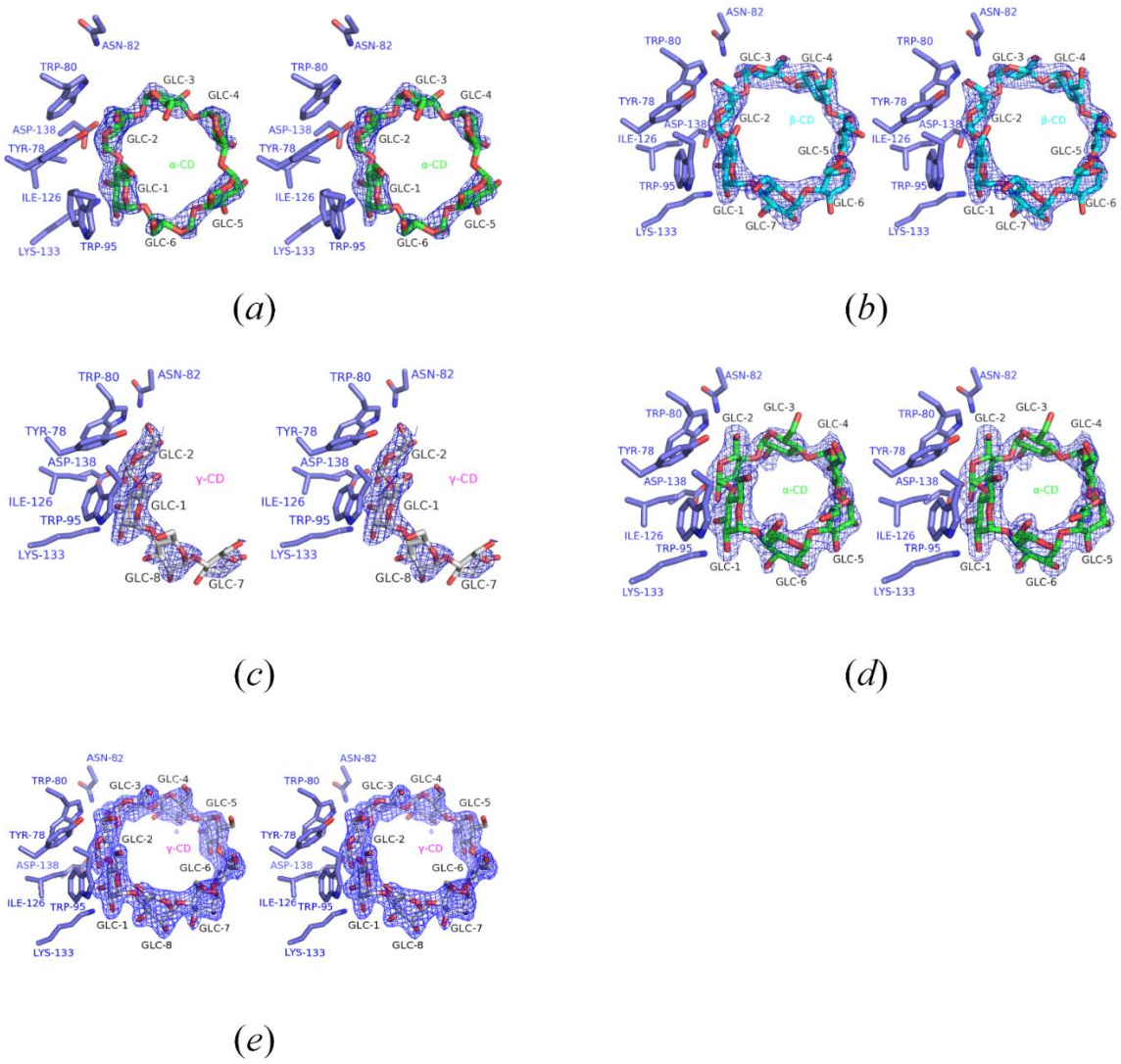

Figure 3 Stereo representation of the comparison of the binding mode in CBM41: (*a*) 1 mM α-cyclodextrin complex, (*b*) 1 mM β-cyclodextrin complex, (*c*) 1 mM γ-cyclodextrin complex, (*d*) 10 mM α-cyclodextrin complex and (*e*) 10 mM γ-cyclodextrin complex structure. The purple, green, cyan and grey sticks are binding residues, α-cyclodextrin, β-cyclodextrin and γ-cyclodextrin, respectively. The density maps show blue mesh lines (2*F*o-*F*c 1.0 σ).

Table 4. Interaction between residues of CBM41 and CDs. Hydrogen bond, C-C clash contacts and C-C contacts distances were in the ranges of 2.45 Å to 3.24 Å, 3.25 Å to 3.94 Å and 3.95 Å to 4.44 Å, respectively. Distances were calculated using Contact from the CCP4 program suite (Collaborative Computational Project, Number 4, 1994). The complex structures observed the C-C contacts and C-C clash contacts were written in parentheses. The apostrophe indicates a residue in the symmetric molecule.

Sugar atom	Protein atom	1 mM α-CD	1 mM β-CD	1 mM γ-CD	10 mM α-CD	10 mM γ-CD	C-C contacts	C-C Clash contacts
GLC 1								
O3	Lys133 NH	2.80	3.04	2.64	2.91	2.68	Trp95	Trp95
O2	Lys133 NH		2.91	3.23	3.18	3.14	Lys133 (1α,1β,1γ,10γ)	Lys133
GLC 2								
O6	Tyr78 OH	2.67	2.59	3.07	2.94		Tyr78 (1β,1γ,10α,10γ)	Tyr78 (1α,1β,10γ)
O2	Asp138 OD1	2.95	3.19	3.21	2.88	2.93	Trp80	Trp80 (1α,1γ,10α,10γ)
O2	Asp138 OD2	3.07		2.80	3.08	2.77	Trp95 (1β, 10γ)	Ile126 (1α,1β,10α,10γ)
O3	Asp138 OD2		2.74	3.10	2.64	2.67	Ile126 (1β,1γ) Asp138 (1α,1γ,10α)	Asp138 (1α,10α,10γ)
GLC 3								
O2	Trp80 NE2		2.94				Trp80 (1β,10γ)	
O2	Trp80 NE1					3.03	Asn82 (1β,10γ)	Trp80 (10γ)
O2	Asn82 ND2		3.00			3.22	Asp138 (1β)	
GLC 4								
GLC 5								
O3	Asp594’ OD1	3.19					Gln593’ (1α)	Gln593’ (1α,10α)
GLC 6								
O2	Asp594’ OD1	2.66 2.89			2.78		Gln593’ (1α,1β,10α)	
O3	Asp594’ OD1		3.02				Asp594’ (1α,10α)	Gln593’ (1β,10γ)
O3	Gln455’ NE2		2.71				Glu404’ (10γ)	
O6	Gln593’ NE2		2.97					
GLC 7								
O2	Asp594’ OD1		2.47					
O3	Gln455’ NE2			2.74		2.64	Gln593’ (1β,1γ,10γ)	Asp594’ (1β)
O3	Asp594’ OD1					2.78	Asp594’ (1β,1γ,10γ)	
O6	Wat			3.06				
GLC 8								
O2	Asp594’ OD1			2.75		2.57	Gln593’ (10γ) Asp594’ (10γ)	

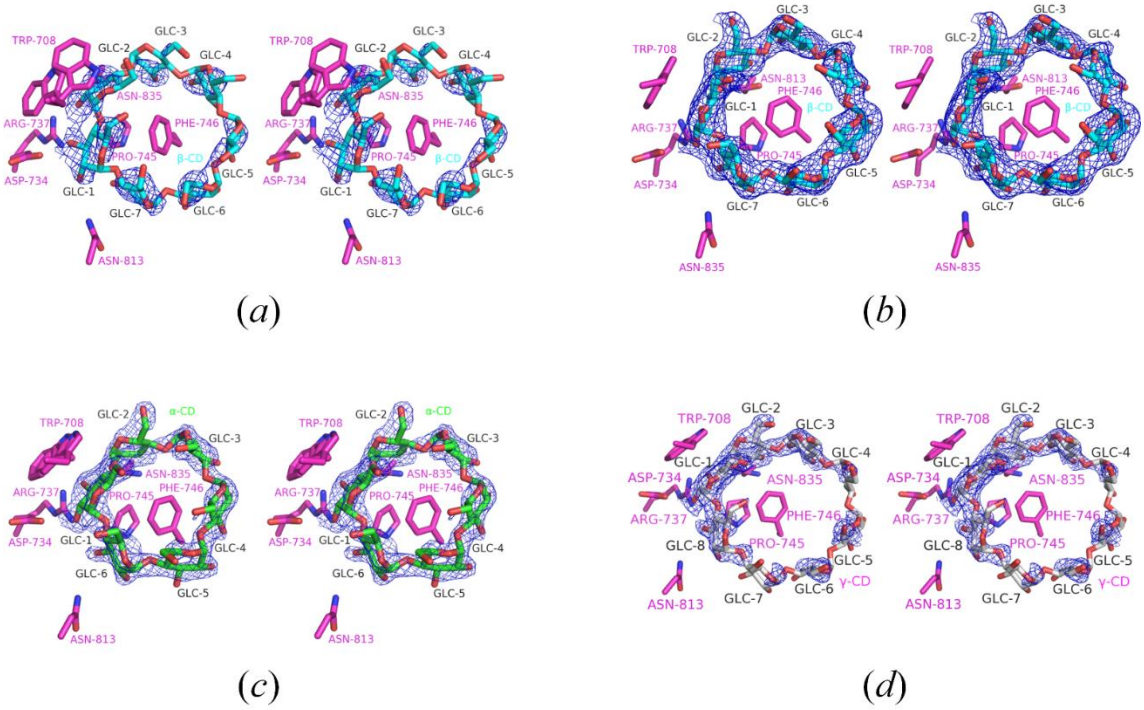

Figure 4 Stereo representation of the comparison of the binding mode in the active site: (*a*) 0.1 mM β-cyclodextrin complex, (*b*) 1 mM β-cyclodextrin complex, (*c*) 10 mM α-cyclodextrin complex and (*d*) 10 mM γ-cyclodextrin complex structure. The magenta, green, cyan and grey sticks are binding residues, α-cyclodextrin, β-cyclodextrin and γ-cyclodextrin, respectively. The density maps show blue mesh lines (2*F*o-*F*c 1.0 σ).

Table 5. Interaction between residues of the active site and CDs. Hydrogen bond, C-C clash contacts and C-C contacts distances were in the ranges of 2.45 Å to 3.24 Å, 3.25 Å to 3.94 Å and 3.95 Å to 4.44 Å, respectively. Distances were calculated using Contact from the CCP4 program suite (Collaborative Computational Project, Number 4, 1994). Arrow shows the water-mediated hydrogen bond. The complex structures observed the C-C contacts and C-C clash contacts were written in parentheses.

Sugar atom	Protein atom	1 mM β-CD	10 mM α-CD	10 mM γ-CD	C-C contacts	C-C Clash contacts
GLC 1						
O2	Asp734 OD2	2.77	2.84	2.67	Trp708	
O2	Arg737 NH2	2.99	2.96	3.05	Asp734	Trp708
O3	Arg737 NH1	2.97	2.74	2.85	Arg737 (10α)	Pro745 (1β)
O6	Wat	2.50	2.56		Pro745 (10α,10γ)	
O6	Wat←Asp709		2.79		Phe746 (10α)	
GLC 2						
O2	Asn835 ND2	3.03				
O2	Asn835 OD1		2.92	3.02		
O3	Asn835 OD1	3.24				
O3	Asn835 ND2		3.19	3.17	Trp708	Trp708 (10α)
O3	Wat→Asp834		3.21		Phe746 (10α,10γ)	Leu678 (10γ)
O6	Wat←Glu706	2.59	2.92			
O6	Wat←Thr642	2.74				
O6	Wat←Ala641		3.05			
GLC 3						
O2	Wat←Asn835	3.12			Phe746 (10α)	Phe746 (10α)
O3	Arg889 NH2			2.67		
GLC 4						
O6	Wat		3.10		Phe746 (10α)	Phe746 (10α)
GLC 5						
					Phe746 (1β, 10α)	Phe746 (10α)
GLC 6						
O3	Wat←Phe746	2.98			Phe746	Phe746 (1β, 10α)
GLC 7						
O2	Wat←Asp738	2.94			Phe746 (1β)	
O3	Wat←Asp738	2.53			Asn813 (1β)	
GLC 8						
					Asn813 (10γ)	

3.5 Interactions between three CDs and Phe746

As mentioned in previous reports (Iwamoto et al., 1993; Iwamoto et al., 1994), β-CD is a stronger inhibitor of KPP compared with other CDs. In the present study, we checked the interaction between CDs and the active site residues. Interestingly, the interaction between CDs and the side chain of Phe746 was remarkably different from the interaction between CDs and other residues. The side chain of Phe746 interacts with the inner ring of the CDs by C-C contacts. In the KPP/α-CD complex structure, six clashes exist even though Phe746 interacts with eighteen atoms (the definition of a C-C clash contact is a contact at a range of distance less than 3.94 Å, while the definition of a C-C contact is a contact at a range of distance between 3.95 and 4.44 Å; Fig. 5*a*). On the other hand, in the KPP/γ-CD complex, the side chain of Phe746 makes only two C-C contacts with the atoms of γ-CD (Fig. 5*c*). In contrast to the α- and γ-CDs, β-CD interacts with Phe746 by seven C-C contacts and only one C-C clash contact (Fig. 5*b*). Because the numbers of hydrogen bonds between the protein residues and the three CDs are almost the same, the optimized C-C contacts between β-CD and the side chain of Phe746 can account for the finding that β-CD exhibited the strongest inhibition in the kinetic and thermodynamic experiments (Iwamoto et al., 1993; Iwamoto et al., 1994). A recent study of *Hv*LD/CD complex structures (Vester-Christensen et al., 2010B) similarly revealed that the inhibition of β-CD was 40-50 times stronger than that of other CDs (Vester-Christensen et al., 2010A). Those authors suggested that the decreased hydrogen bond network and the inclination of the side chain of Phe residue toward the CD ring are both important for the difference of interaction. In the present

study, we showed clearly that the C-C contacts and C-C clash contacts were important for the different interactions between Phe746 of KPP and CDs.

3.6 Effect of F746 mutation

To confirm the effect of Phe746, we constructed an expression system of recombinant *Klebsiella pneumoniae* pullulanase (PulA) and the F746A variant and purified the enzymes. The K_m and k_{cat} values of PulA and the F746A variant against pullulan and the K_i values of CDs were examined as described in Table.6. In contrast to the strong inhibition of β-CD found in PulA (0.48 μM), very weak inhibition of β-CD (833 μM) was found in F746A. There was almost no difference in the K_i values among the three CDs in the case of F746A, revealing the important role of Phe746 in the strong binding of β-CD. Moreover, the K_m and k_{cat} values for the F746A variant were different from those for PulA. Phe746 interacts with glucose of subsite +2. We suggested that the mutation from Phe746 to Ala caused a decrease in the binding affinity and reduced the catalytic activity.

Table 6. Kinetic parameters for pullulan and inhibitor constants (K_i) for cyclodextrins

	Pullulan			α-CD	β-CD	γ-CD
	K_m (μM)	k_{cat} (/s)	k_{cat}/K_m	K_i (μM)	K_i (μM)	K_i (μM)
PulA	18.746	52.0	2.774	15.1	0.48	18.1
F746A	8.446	17.1	2.025	516	833	690

4. Conclusion

In this study, we refined the structures of ligand-free KPP and complexes of KPP with CDs in a newly crystallized space group. These structures revealed the interactions of α-, β- and γ-CDs with CBM41 and with the active site of the A domain. Moreover, analysis of the three-dimensional structures revealed that the interaction between KPP and CDs could be changed by changing the concentration and the type of CDs used for the crystallization. CBM41 bound with the CDs when the concentration of CDs was

more than 1 mM. That is, the concentration of CDs interacting with CBM41 did not depend on the kind of CDs. On the other hand, β-CD bound to the active site when present at a concentration of 0.1 mM, while the α- and γ-CDs bound to the active site only at concentrations of more than 10 mM. These results suggested that the concentration of CDs required for interaction with the active site depends on the kind of CDs, which agrees with the results of the inhibition experiments in solution. The highest inhibition of β-CD (0.48 μM) was attributed to the optimal C-C contacts between the side chain of Phe746 and inner ring of β-CD. The extreme decrease in inhibition of the binding of β-CD to the F746A variant clearly indicated the important role of Phe746 in the binding of β-CD to KPP.

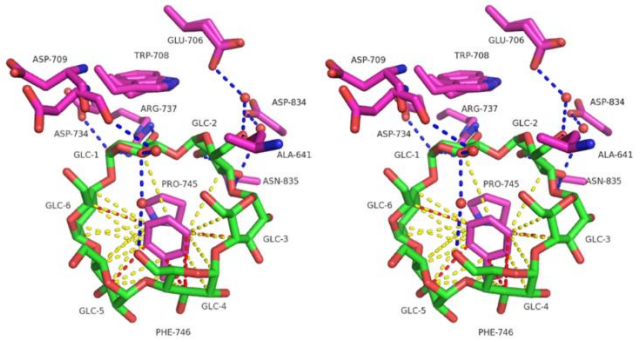

(*a*)

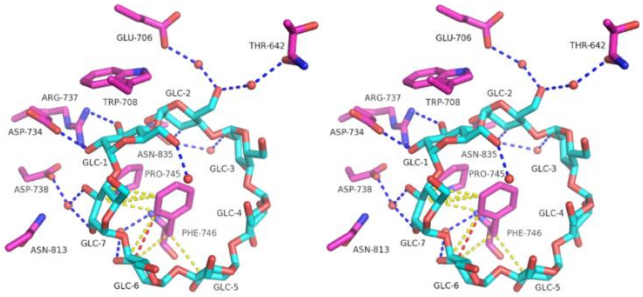

(*b*)

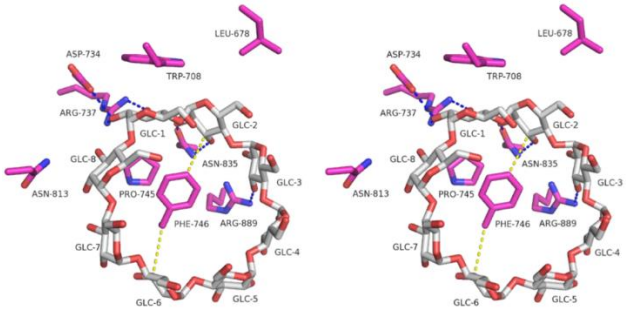

(*c*)

Figure 5 Stereo representation of the comparison of the interaction between cyclodextrin and binding residues: (*a*) α-cyclodextrin, (*b*) β-cyclodextrin and (*c*) γ-cyclodextrin. The magenta, green, cyan and grey sticks are binding residues, α-cyclodextrin, β-cyclodextrin and γ-cyclodextrin, respectively. The red spheres are intermediate water. The blue, yellow and red dashed lines are a hydrogen bond (2.45 – 3.24 Å), C-C contact (3.95-4.44 Å) and C-C clash contact (3.25-3.94 Å), respectively.

References

Abdullah, M. & French, D. (1970). *Arch. Biochem. Biophys.* **137**, 483-493.

Adachi, M., Mikami, B., Katsube, T. & Utsumi, S. (1998). *J. Biol. Chem.* **273**, 19859-19865.

Adams, P. D., Grosse-Kunstleve, R. W., Hung, L.-W., Ioerger, T. R., McCoy, A. J., Moriarty, N. W., Read, R. J., Sacchettini, J. C., Sauter, N. K. & Terwilliger, T. C. (2002). *Acta Cryst. D* **58**, 1948-1954

Bender, H. & Wallenfels, K. (1961). *Biochem. Z.* **334**, 79.

Collaborative Computational Project, Number 4. (1994). *Acta Cryst. D* **50**, 760-763.

Cremer, D. & Pople, J.A. (1975). *J. Am. Chem. Soc.* **97**, 1354-1358.

DeLano, W.L. (2002). The PyMOL molecular graphics system. DeLano Scientific, San Carlos, CA.

East, A., Mechaly, A E., Huysmans, G H., Bernarde, C., Tello-Manigne, D., Nadeau, N., Pugsley, A P., Buschiazzo, A., Alzari, P M., Bond, P J. & Francetic, O. (2016). *Structure*, **24**, 92-104.

Emsley, P. & Cowtan, K. (2004). *Acta Cryst. D* **60**, 2126-2132.

Gourlay, L. J., Santi, I., Pezzicoli, A., Grandi, G., Soriani, M. & Bolognesi, M. (2009). J. Bacteriol. 191, 3544-3552.

Harada, T. , Misaki, A. , Akai, H. , Yokobayashi, K. & Sugimoto, K. (1972). *Biochim. Biophys. Acta,* **268**, 497-505.

Hondoh, H., Kuriki, T. & Mastuura, Y. (2003). *J. Mol. Biol.* **326**, 177-188.

Hytönen, J., Haataja, S. & Finne, J. (2003). *Infrect. Immun.* **71**, 784-793.

Imberty, A., Chanzy, H., Pèrez, S., Bulèon, A., & Tran, V. (1988). *J. Mol. Biol.* **201**, 365-378.

Iwamoto, H., Ohmori, M., Ohno, M., Hirose, J., Hiromi, K., Fukada, H., Takahashi, K., Hashimoto, H. & Sakai, S. (1993). *J. Biochem.* **113**, 93-96.

Iwamoto, H., Ohno, M., Ohmori, M., Hirose, J., Tanaka, A., Sakai, S. & Hiromi, K. (1994). *J. Biochem.* **116**, 1264-1268.

Katsuya, Y., Mezaki, Y., Kubota, M. & Matsuura, Y. (1998). *J. Mol. Biol.* **281**, 885-897.

Lammert van Bueren, A., Ficko-Blean, E., Pluvinage, B., Hehemann, J. H., Higgins, M. A., Deng, L., Ogunniyi, A. D., Stroeher, U. H., El, Warry, N., Burke, R. D., Czjzek, M., Paton, J. C., Vocadio, D. J. & Boraston, A. B. (2011). *Structure.* **19**, 640-651.

Larson, S. B., Day, J. S. & McPherson, A. (2010). *Biochemistry*, **49**, 310-315.

Lesk, A. M. (1991). *Protein Architecture: A Practical Approach*, IRL Press, Oxford.

Lombard, V., Golaconda Ramulu, H., Drula, E., Coutinho, P. M. & Henrissat, B. (2014). *Nucleic Acids Res*. **42**, D490-D495.

Manners, D. (1997). *J. Appl. Glycosci.* **44**, 83-85.

Marshall, J. J. (1973). *FEBS. Lett.* **37**, 269-273.

Malle, D., Itoh, T., Hashimoto, W., Murata, K., Utsumi, S. & Mikami, B. (2006). *Acta Cryst. F* **62**, 381-384.

Mikami, B., Iwamoto, H., Malle, D., Yoon, H.-J., Demirkan-Sarikaya, E., Mezaki, Y. & Katsuya, Y. (2006). *J. Mol. Biol.* **359**, 690-707.

Mikami, B., Hehre, EJ., Sato, M., Katsube, Y., Hirose, M., Morita, Y. & Sacchettini, JC. (1993). *Biochemistry*. **32**, 6836-6845.

Møller, M. S., Windahl, M. S., Sim, L., Bojstrup, M., Abou Hachem, M., Hindsgaul, O., Palcic, M., Svensson, B. & Henriksen, A. (2015A). *J. Mol. Biol.* **427**, 1263-1277.

Møller, M. S.,Vester-Christensen, M. B., Jensen, J. M., Hachem, M. A., Henriksen, A. & Svensson, B. (2015B). *J. Biol. Chem.* **290**, 12614-12629.

Murshudov, G. N., Vagin, A. A. & Dodson, E. J. (1997). *Acta Cryst. D* **53**, 240-255.

Murshudov, G. N., Skubak, P., Lebedev, A. A., Pannu, N. S., Steiner, R. A., Nicholls, R. A., Winn, M. D., Long, F. & Vagin, A. A. (2011). *Acta Cryst. D* **67**, 355-367.

Otwinowski, Z. & Minor, W. (1997). *Methods Enzymol.* **276**, 307-326.

Rejzek, M., Stevenson, C. E., Southard, A. M., Stanley, D., Denyer, K., Smith, A. M., Naldrett, M. J., Lawson, D. M. & Field, R. A. (2011). *Mol. Biosyst.* **7**, 718-730.

Schmidt, A. K., Cottaz, S., Driguez, H. & Schulz, G. E. (1998). *Biochemistry*. **37**, 5909-5915.

Sim, L., Beeren, S. R., Findinier, J., Dauvillèe, D., Ball, S. G., Henriksen, A. & Palcic, M. M. (2014). *J. Biol. Chem.* **289**, 22991-23003.

Szejtli, J. (1998). *Chem. Rev.* **98**, 1743-1754.

Turkenburg, J. P., Brzozowski, A. M., Svendsen, A., Borchert, T. V., Davies, G. J. & Wilson, K. S. (2009). *Protein*. **76**, 516-519.

Uitdehaag, J. C., Kalk, K. H., van Der Veen, B. A., Dijkhuizen, L. & Dijkstra, B. W. (1999). *J. Biol. Chem.* **274**, 34868-34876.

Vagin, A. & Teplyakov, A. (1997). *J. Appl. Cryst.* **30**, 1022-1025.

Vester-Christensen, M. B., Hachem, M. A., Naested, H. & Svensson, B. (2010A). *Protein. Expr. Purif.* **69**, 112-119.

Vester-Christensen, M. B., Abou, Hachem, M., Svensson, B. & Henriksen, A. (2010B). *J. Mol. Biol.* **403**, 739-750.

Van Bueren, A. L., Higgins, M., Wang, D., Burke, R. D. & Boraston, A. B. (2007). *Nat. Struct. Mol. Biol.* **14**, 76-84.

Xu, J., Ren, F., Huang, C. H., Zheng, Y., Zhen, J., Sun, H., Ko, T P., He, M., Chen, C. C., Chan, H. C., Guo, R. T., Song, H. & Ma, Y. (2014). *Protein*. **82**, 1685-1693.

Yokobayashi, K., Akai, H., Sugimoto, T., Hirao, M., Sugimoto, K. & Harada, T. (1973). *Biochim. Biophys. Acta,* **293**, 197-202.

Yokota, T., Tonozuka, T., Shimura, Y., Ichikawa, K., Kamitori, S. & Sakano, Y. (2001). *Biosci. Biotechnol. Biochem.* **65**, 619-626.

Chapter 2

Relationship between induced-fit loop and activity of *Klebsiella pneumoniae* pullulanase

1. Introduction

Starch hydrolases are classified to 153 glycoside hydrolase (GH) families in the database of carbohydrate active enzyme (CAZy; http://www.cazy.org/, Lombard et al., 2014) according to their amino acid sequence. Amylases are the enzymes that degrade for α-glucan such as starch, glycogen and pullulan. GH family 13 is large family in GH families known as α-amylase family, divided 42 subfamilies according to their sequence homology and biochemical property. Pullulanase (EC 3.2.1.41) is enzyme that hydrolyzes α-1,6-glycosidic linkage of α-glucan (Hii et al., 2012, Bertoldo & Antranikian, 2002, Domań-Pytka & Bardowski, 2004), divided in subfamily 12-14 of GH13 family (GH13_12, GH13_13, GH13_14; Stam et al., 2006). According to phylogenetic classification, GH13_13 is branched from GH13_14. Compared with GH13_13 based on structural-based sequence alignment, there are three lacks (the parts of L2, L6b and L8) and insert (between α1b and α1) in GH13_14 (Stam et al., 2006, Mikami et al., 2006). To date, we reported ligand-free, substrate-analogs (G1, G2, G3, G4 and isoG2) and α-, β-, γ-cyclodextrins complex structures of pullulanase from *Klebsiella pneumoniae* produced by Hayashibara Co. (hereinafter called KPP; Mikami et al., 2006, Saka et al., 2018). KPP is an enzyme derived from the strain of *Klebsiella pneumoniae* ATCC 9621 and consists of five domains (CBM41, N2, CBM48, A and C). A domain included active site of KPP consists of $(\beta/\alpha)_8$-barrel structure and belongs to GH13_13. Catalytic residues are conserved Asp677 as nucleophile, Glu706 as acid/base and Asp834 as transition-state stabilizer. There are highly conserved regions in GH13 family enzymes, region II, III and IV include the residues of

Asp677, Glu706 and Asp834, respectively (Yamashita et al., 1997, Svensson 1994, Kuriki & Imanaka, 1999, Janeček, 2002). Attempting structural-based sequence alignment of conserved regions of starch debranching enzymes included in GH13_13, we revealed there is difference in conserved region II (Fig.1*a*). The sequence of region II of KPP is GFRFDLM"L"Y, however, the sequence of other GH13_13 enzymes are GFRFDLM"G"Y(H). In contrast to KPP, the residue 680 in the pullulanase of another strain of *Klebsiella pneumoniae* ATCC9621 (hereinafter called PulA) is Gly, same as the most of GH13_13 enzymes.

KPP is reported to perform an induced-fit motion of the active site loop (resid. 706-710) included in conserved region III upon binding of malto-oligo-saccharides (Mikami et al., 2006, Saka et al., 2018). In contrast to KPP, the loop conformation of limit dextrinase from *Hordeum vulgare* (*Hv*LD; Vester-Christensen et al., 2010, Møller et al., 2015) was reported to be unchanged between ligand-free structure and complex structure. In KPP structures, the conserved region II region including the mutated Leu680 is located just behind the above-mentioned loop (Fig.1*b*, *c*), suggesting that the conformational change of the active site loop in KPP is caused by Leu680. Though there is one more different residue, Asn299 in KPP which is altered to be Ser299 in PulA, doesn't relate with activity as it is located in N2 domain apart from the active site.

In this paper, pullulanase (PulA-G680) and its mutant pullulanase (PulA-L680) from *Klebsiella pneumoniae* ATCC 9621 strain were expressed in *Escherichia Coli*. The crystal structure analysis and functional analysis of these enzymes elucidated the structural mechanism of the induced fit motion of KPP and PulA.

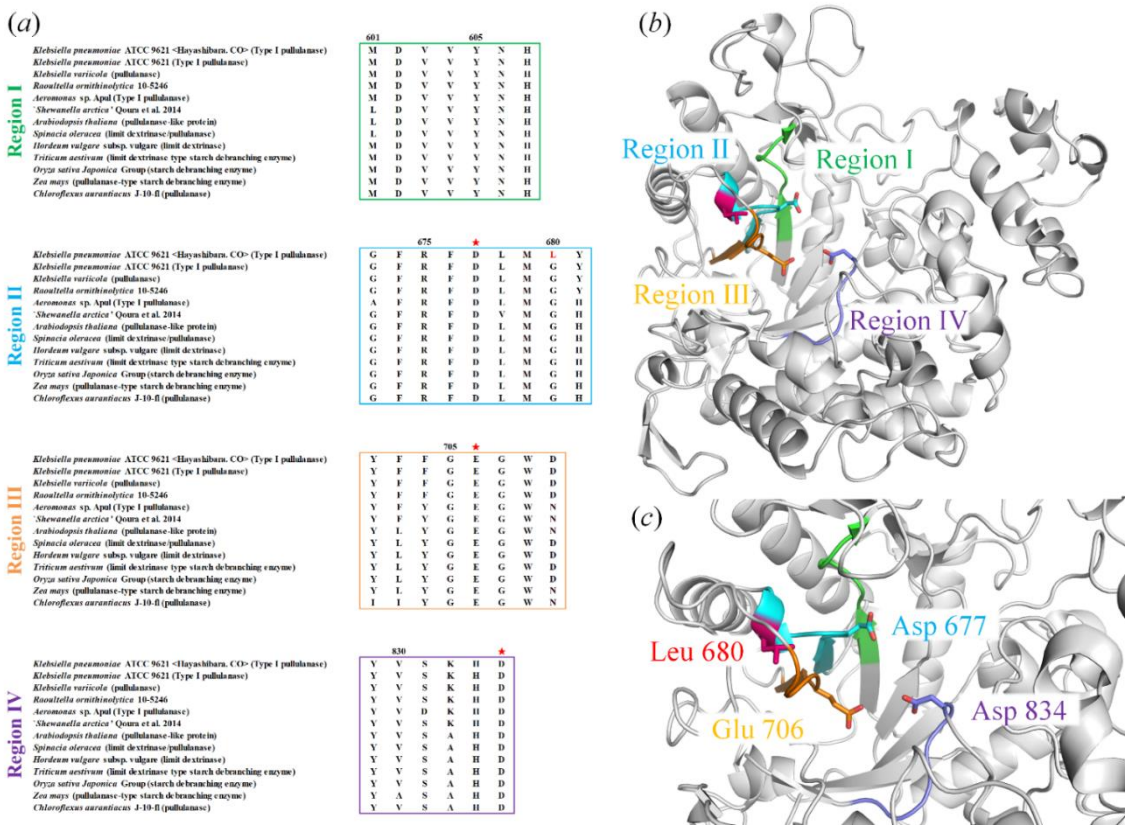

Figure 1 (*a*) Structural based sequence alignments of conserved region I ~ IV in starch debranching enzymes from GH13 subfamily 13. Region I ~ IV are surrounded with green, cyan, orange and purple boxes, respectively. Red stars show conserved catalytic residues. (*b*, *c*) Structure of A domain of KPP (PDB code: 2FGZ). Region I ~ IV are showed with green, cyan, orange and purple, respectively. Cyan, red, orange and purple sticks show Asp677, Leu680, Glu706 and Asp834, respectively.

2. Experimental Procedures

2.1 Site-directed mutagenesis

Mutant PulA-L680 gene was constructed by a double PCR method. The PCR reaction was performed in a reaction volume totaling 50 μL containing 5 U Pfu Turbo Hotstart DNA polymerase (Agilent Technologies), 10 × cloned Pfu reaction buffer, 500 μM dNTP, 400 nmol/mL of two synthesized mutagenesis primers and 25 ng/μL pCold-TF vector (Takara Bio Co.) including the PulA-G680 gene, which had been previously constructed (Saka et al., 2018). The above-mentioned primers were using following forward primer; 5'-TTCGACCTGATG**CTG**TACCACCCGAAAGC-3' and reverse primer; 5'-

TGCGCTTTCGGGTGGTA**CAG**CATCAGGTC-3'. PCR reaction was using T100™ thermal cycler (BIO-RAD Laboratories, Inc.). A condition is two steps; first step is denaturation for 10 sec at 92℃, annealing for 30 sec at 55℃ and elongation 20 min at 68℃, for 10 cycles, second step is denaturation for 10 sec at 92℃, annealing for 30 sec at 55℃ and elongation 20 min 10 sec at 68℃, for 20 cycles. After PCR reaction, reaction product had treated by *Dpn*I (Takara Bio Co.) at 37℃ for 1 hour. The constructed mutant vector was transformed into *Escherichia coli* strain BL21 (Takara Bio Co.) using heat shock method.

2.2 Expression and purification

Expression system of PulA-G680 and G680L mutant were used reported previous. Crude solution was applied onto Cobalt ion immobilized chelating Sepharose Fast Flow (GE Healthcare Life Sciences) equilibrated by 500 mM sodium chloride containing 50 mM Tris-HCl buffer (pH 8.0). Protein solution were eluted by 500 mM sodium chloride and 200 mM imidazole containing 50 mM Tris-HCl buffer (pH 8.0). Eluted solution was changed to PBS solution. This protein is fusion protein of His-tag containing Trigger factor, therefore fusion protein had treated by 10 U thrombin (GE Healthcare Life Science) at 293 K in 3 days. After the treatment, protein solution was changed to 500 mM sodium chloride containing 50 mM Tris-HCl buffer (pH 8.0), reapplied onto Cobalt ion immobilized chelating Sepharose Fast Flow, collected flow through fraction. Collected fraction was changed to 50 mM Tris-HCl buffer (pH 8.0), later applied onto MonoQ 10/100 GL (GE Healthcare Life Sciences) equilibrated by same buffer. Protein solution was eluted with a linear gradient of sodium chloride from 0 to 500 mM. Collected fraction was changed to 50 mM sodium acetate buffer (pH 6.0) and concentrated to 9 mg/mL using Vivaspin® 20 (sartorius stedim biotech).

2.3 Crystallization and data collections

Crystals of PulA-G680 and PulA-L680 has made using the method of previous report (Mikami et al., 2006). Data collections of ligand-free structure were used covered crystals by reservoir solution added 20% glycerol as cryoprotectant. Data collections of maltotriose (G3)-complex

structure were performed after soaking the ligand-free crystals to the reservoir solution containing 300 mM maltotriose and 20% glycerol as a cryoprotectant. Diffraction pattern of ligand-free and G3-complex crystals were checked using a Bruker Hi-Star multiwire area detector at 100 K and using Cu Kα rotation generated by a Mac Science M18XHF rotating anode generator. Diffraction data were collected by CCD and imaging-plate detectors in SPring-8 (Hyogo, Japan) using beamlines of BL26B1 and BL44XU. The collected images were processed by HKL2000 program (Otwinowski & Minor, 1997).

2.4 Structural determination and Refinement

The crystal structures of ligand-free and G3-complexes were determined by molecular replacement method using atomic coordinates of KPP (PDB code; 2FHC) as a search model with the MOLREP (Vagin & Teplyakov, 1997) from the CCP4 program suite (Collaborative Computational Project, Number 4, 1994). The structures were refined with REFMAC5 (Murshudov et al., 1997, Murshudov et al., 2011) from the CCP4 program suite and phenix.refine from PHENIX program suite (Adams et al., 2002) after model rebuilding with COOT program (Emsley & Cowtan, 2004) as shown in Table 1. Ribbon and stick models and electron density maps were prepared using PyMOL (DeLano, 2004). Cremer-Pople parameters were calculated by Web-site calculator (http://enzyme13.bt.a.u-tokyo.ac.jp/CP/) based on the method of Cremer-Pople (Cremer & Pople, 1975). Distances for hydrogen bonds and C-C contacts were calculated using Contact from the CCP4 program suite (Collaborative Computational Project, Number 4, 1994).

2.5 Activity study

Activities of PulA-G680 and PulA-L680 were measured using a modified Park-Johnson method (Saka et al., 2018). The Michaelis constant (K_m) and rate of a reaction (k_{cat}) were measured for the reaction mixture containing the substrate pullulan (0-0.03%), PulA-G680 (6.0×10^{-10} M) or PulA-L680 (6.0×10^{-10} M), in 0.05 M sodium acetate buffer (pH 5.6) at 25°C.

Table 1. Data Collections and Refinement Statistics/

substrate analog (mM)	PulA-G680 ligand-free	PulA-G680/G3 (300mM)	PulA-L680 ligand-free	PulA-L680/G3 (300mM)
A. Diffraction data				
X-ray source	SPring-8/BL26B1	SPring-8/BL26B1	SPring-8/BL44XU	SPring-8/BL26B1
Detector	mx225HE	R-AXIS V	mx300HE	mx225HE
Wavelength (Å)	1.0	1.0	0.9	1.0
Resolution range (Å)	50.00 – 1.30 (1.34 – 1.30)	50.00 – 1.50 (1.55 – 1.50)	50.00 – 1.84 (1.90 – 1.84)	50.00 – 1.64 (1.70 – 1.64)
Space group	*P*1	*C*2	*P*1	*C*2
Unit cell parameters				
a, b, c (Å)	60.4, 80.3, 127.7	148.9, 60.1, 133.8	60.2, 80.2, 127.3	148.9, 60.1, 134.0
α, β , γ (°)	96.7, 102.3, 112.1	90.0, 114.7, 90.0	94.9, 103.0, 112.0	90.0, 114.7, 90.0
Unique reflections	495665 (46251)	170223 (16219)	181784 (17267)	131547 (12890)
Multiplicity	3.8 (2.7)	5.8 (5.8)	2.7 (2.7)	3.8 (3.5)
Completeness (%)	94.4 (88.0)	98.5 (94.8)	97.5 (93.3)	99.8 (98.6)
Mean $I/\sigma(I)$	20.1 (3.5)	26.4 (6.1)	19.7 (8.8)	16.9 (3.6)
Wilson *B*-factor (Å^2)	15.0	15.6	16.0	16.9
R_{merge} (%)	5.2 (33.4)	5.6 (37.0)	4.7 (13.6)	6.9 (33.9)
R_{meas} (%)	5.8 (41.3)	6.1 (40.6)	6.0 (17.5)	8.1 (39.9)
R_{pim} (%)	2.6 (24.0)	2.5 (16.6)	3.7 (10.7)	4.1 (20.9)
$CC_{1/2}$ (%)	99.9 (84.9)	99.9 (96.6)	99.7 (96.8)	99.7 (92.0)
B. Refinement statistics				
Resolution range used refinement	39.3 – 1.30 (1.31 – 1.30)	47.2 – 1.50 (1.52 – 1.50)	38.7 – 1.84 (1.86 – 1.84)	38.3 – 1.64 (1.66 – 1.64)
R_{work} (%)	12.8 (18.1)	13.0 (16.9)	16.4 (20.5)	16.5 (20.8)
R_{free} (%)	15.3 (21.9)	16.0 (19.9)	18.9 (27.7)	18.4 (23.7)
Number of Ca^{2+}/Mg^{2+}/Glc/Gol/Ace	1/22/0/0/8	0/4/6/4/1	9/1/0/2/0	2/2/6/3/0
water	3132	1159	1552	801
Protein residues	2098	930	2097	917
R.m.s.d., bond lengths (Å)	0.008	0.010	0.010	0.006
R.m.s.d., bond angles (°)	0.96	1.01	1.07	0.80
Ramachandran favored (%)	98.2	98.2	97.8	98.2
Rotamer outliers (%)	1.33	1.25	1.46	1.55
Clashscore	3.55	3.59	4.47	2.10
Average *B*-factor (Å^2)	22.9	28.6	22.4	24.6
PDB ID	6J33	6J34	6J35	6J4H

3. Results and discussion

3.1 Measurement of kinetic parameters

Activity assay of PulA-G680 and PulA-L680 toward pullulan were shown in Table. 2. Activity parameters of PulA-G680, k_{cat}, K_m and k_{cat}/K_m, were 77.3 s^{-1}, 32.1 μM and 2.41 s^{-1}μM, respectively. On the other hand, activity parameters of PulA-L680, k_{cat}, K_m and k_{cat}/K_m, were 29.9 s^{-1}, 48.6 μM and 0.62 s^{-1}μM, respectively, that are similar to the values of KPP (Iwamoto et al, 1993). These results indicate that mutation of PulA from Gly680 to Leu680 reduced the reaction velocity and substrate affinity, suggesting that PulA-L680 has similar property to KPP (Saka et al., 2018).

Table 2. Kinetic parameters of PulA-G680, PulA-L680 and KPP.

	k_{cat} (s^{-1})	K_m (μM)	k_{cat}/K_m
PulA-G680	77.3	32.1	2.41
PulA-L680	29.9	48.6	0.62
KPP	37.3	64.3	0.58

3.2 Overall structures

The structures of ligand-free and G3-complex of PulA-G680 and PulA-L680 were refined at 1.30 ~ 1.83 Å resolution (Table 1). Space group of ligand-free-form is *P*1 containing two molecules, and that of G3-complex is *C*2 containing one molecule, although the crystals were made in the same crystallization conditions. As the alternation of space group is found in both crystals of PulA-G680 and PulA-L680, the change of the space group seems to be caused by the binding of G3. Though PulA-G680 and PulA-L680 contain residues from 32 to 1083, we could not put residues 64-69 of chain A at ligand-free structure of PulA-G680, residues of 63-70 of chain B at ligand-free structure of PulA-L680, residues of 38-159 of G3 complex of PulA-G680 and residues of 38-172 of G3 complex of PulA-L680 owing to unclear density map. In the N-terminal, we put the model of Met31 of chain B at the ligand-free structures of PulA-G680 and PulA-L680, which was derived from sequence of *Nde*I. In *P*1 crystals of the ligand-free enzymes, there is no difference between the two molecules in an asymmetric unit as revealed by root-mean-square deviation (r.m.s.d) of 0.104 Å (PulA-G680) and 0.072 Å (PulA-L680), except for CBM41. The relative position of the N-terminal domain, CBM41, is different between the two molecules in the asymmetric unit, rotating approximately 10° (ligand-free PulA-G680) and 7° (ligand-free PulA-L680) which may cause the difference of space group *P*1 (ligand-free) and *C*2 (G3 complex). Moreover, the r.m.s.d values between ligand-free enzyme and G3-complex are 0.181 Å (PulA-G680 chain A of ligand-free structure), 0.167 Å (PulA-G680 chain B of ligand-free structure), 0.107 Å (PulA-L680 chain A of ligand-free structure) and 0.093 Å (PulA-L680 chain B of ligand-free structure), suggesting the structural identity even between ligand-free and G3 complex. Two G3 molecules are binding to subsite +2, +1 and 0', and -1 ~ -3, of

PulA-G680 (Fig.2 *a*) and PulA-L680 (Fig.2 *b*), as reported in the case of KPP. Sugar conformation of all glucose residues bound to the active site are $^4C_1$ pyranoside forms, according to the calculated Cremer-Pople parameter (Supplemental Table 1). Furthermore, the values of torsion-angle of α-1,4-glycosidic linkage (Φ = 85.61~103.71 and Ψ = -132.3~-152.22), are in region of low-energy of isoenergy map as is the case of KPP (Supplemental Table 1, Imberty et al., 1988).

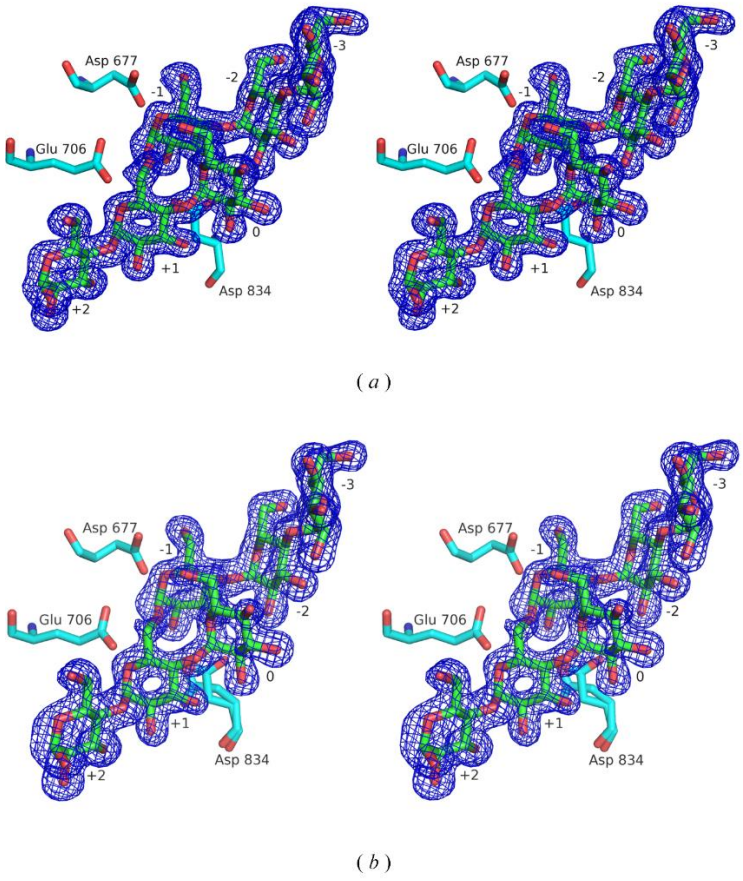

Figure 2 Stereo representations of maltotriose molecules bound to active site of PulA-G680 (*a*) and PulA-L680 (*b*). Green and cyan sticks show maltotriose molecules and catalytic residues, respectively. The sugar 2*F*o-*F*c maps are contoured at 1.0 σ level and colored in blue.

Table 3. Sugar puckering parameters and torsion angles. The Table is Cremer-Pople parameters and torsion angles for maltotriose molecules bound to active site. Cremer-Pople parameters were calculated using a Web-site calculator (http://enzyme13.bt.a.u-tokyo.ac.jp/CP/). The torsion angles were calculated using the COOT program (Emsley and Cowtan, 2004). Torsion angles were defined as O5 – C1 – O4' – C4' (Φ) and C1 – O4' – C4' – C5' (ψ) between glucose molecules of the side of non-reducing end (include C1 atom) and glucose molecules of the side of reducing end (include O4 atom; dash number).

		+2	+1	0	-1	-2	-3
	Φ (°)	210.268	270.745	117.646	172.924	242.811	257.772
	Θ (°)	7.062	7.061	0.886	16.390	5.607	1.060
PulA	Q	0.569	0.594	0.584	0.607	0.583	0.566
G680	conformation	$^4C_1$	$^4C_1$	$^4C_1$	$^4C_1$	$^4C_1$	$^4C_1$
	Φ (°)	102.77	101.30		85.61	99.52	
	Ψ (°)	-132.30	-131.48		-155.75	-141.17	

	Φ (°)	248.041	289.720	45.549	123.135	259.581	269.902
	Θ (°)	5.995	6.464	5.629	11.731	3.402	1.296
PulA	Q	0.575	0.608	0.584	0.590	0.607	0.578
G680L	conformation	$^4C_1$	$^4C_1$	$^4C_1$	$^4C_1$	$^4C_1$	$^4C_1$
	Φ (°)	103.71	102.16		87.69	98.65	
	Ψ (°)	-138.91	-132.36		-152.22	-142.19	

3.3 Relationship between the side-chain of 680 and the motion of the loop

Figure 3 shows the conformation of the loop (706-710) and the side-chain of 680. Supplemental Table 2 and Figure 4 represent the main-chain dihedral angles and Ramachandran plot for residues 706-710 in PulA-G680 and PulA-L680. As mentioned above, the crystals of ligand-free PulA-G680 and PulA-L680 contains two molecules in the asymmetric unit. Conformation of the loop of PulA-G680/G3 did not change from that of ligand-free PulA-G680 (Supplemental Table 2, Fig. 3 *a*, *b*, and Fig. 4 *a*, *b*). These loop conformations are same conformation of G3-complex structure of KPP (Fig. 3 *d*). Though the loop conformation of chain A of PulA-L680 is the almost same as that of PulA-G680 ligand-free (Supplemental Table 2), the loop conformation of chain B of the ligand free PulA-L680 has alternate conformations, one is the same conformation as that of PulA-G680 (Supplemental Table 2 and Fig. 3 *c*) and the other is the almost the same as the ligand-free KPP structure (Supplemental Table 2, Fig. 3 *c* and Fig. 4 *e*). There is also difference of dihedral angles of the loop between the ligand-free (Alt. B of chain B) and G3-complex structure of PulA-L680 (Supplemental Table 2, Fig. 3 *d* and Fig. 4 *c*). The loop structure of ligand-free in Alt. B of chain B of PulA-L680 is similar to the loop structure of the ligand-free of KPP (Supplemental Table 2 and Fig. 4 *f*). These results suggested

that the existence of Leu680 induces the conformation change of the loop included residues 706-710 in the ligand-free state. The hydrogen bond interactions between residue 680 and the loop residues of 706-710 were depicted in Table 3. In PulA-G680 structures, O of Gly680 forms hydrogen bond with OG atom of Ser710, both in the ligand-free and G3-complex. Moreover, in G3-complex structures of PulA-G680 and PulA-L680, N of residue 680 forms hydrogen bond with O of Glu706. O of residue 680 in chain A and Alt. A of chain B of ligand-free PulA-L680 makes a hydrogen bond with OG atom of Ser710 as is the case of PulA-G680. These results indicated that the structural change of Alt. B of chain B in the ligand-free PulA-L680 has no hydrogen bond to any atoms of the loop residues.

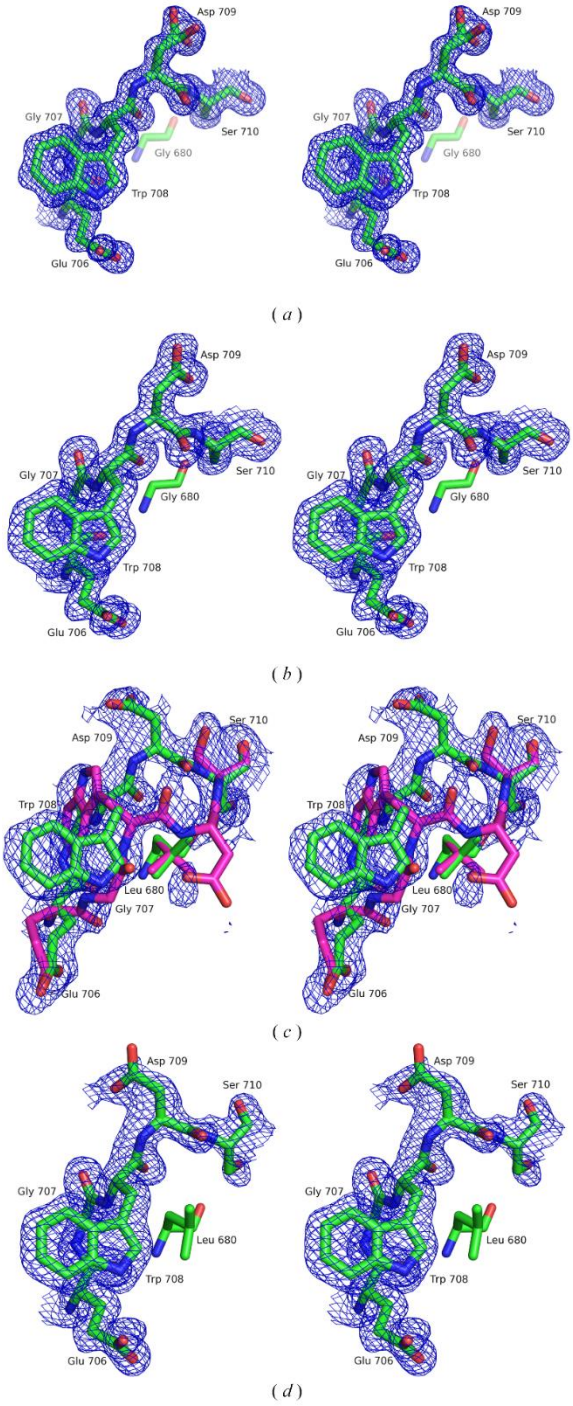

Figure 3 Stereo representations of residue 680 and 706-710 loop of chain A in ligand-free structure of PulA-G680 (*a*), G3-complex structure of PulA-G680 (*b*), chain B in ligand-free structure of PulA-L680 (*c*) and G3-complex structure of PulA-L680 (*d*), respectively. Green sticks show the residues of 680 and loop 706-710 (*a*, *b*, *c*, *d*). The loop 2*F*o-*F*c maps are contoured at 1.0 σ level and coloured in blue (*a*, *b*, *c*, *d*). Green and magenta sticks show alternate conformation A and B of the residues of 680 and loop 706-710 (*c*). The 2*F*o-*F*c maps around the loop are contoured at 0.6 σ level and coloured in blue (*c*).

Figure 5 shows the C-C contacts of these regions divided by C-C clash and C-C interactions. In PulA-G680, Gly680 interacts with only Ser710 in both ligand-free and G3-complex structures (Fig. 5 a and b), whereas Leu680 of PulA-L680 forms C-C clash and C-C interactions to many residues of the mobile loop (Fig. 5 c, d and e). Among them, Leu680 in alternate conformation B of chain B in ligand-free structure forms C-C clash interactions with Gly707, Trp708 and Ser710, and C-C interactions with Glu706, Trp708 and Ser710 (Fig. 5 c and d). Comparison of these interactions with those of PulA-G680 and KPP clearly shows that the ligand-free PulA-G680 has the almost the same structure with G3-complex of KPP in contrast to the structure of the ligand-free PulA-L680 (Alt. B in chain B) which has distorted main-chain dihedral angle (Fig. 6). These differences in the interaction between residue 680 and residues 706-710 included in the loop have an impact on the conformation change of mobility loop.

Table 4. Dihedral angles of residues 706-710. Dihedral angle parameters were calculated using a Web-site calculator (http://cib.cf.ocha.ac.jp/bitool/DIHED/). Dihedral angles were defined as C^{n-1}-N^n-$C\alpha^n$-$C\alpha^n$ (Φ) and N^n-$C\alpha^n$-C^n-N^{n+1} (Ψ).

		Glu706		Gly707		Trp708		Asp709		Ser710	
		Φ	Ψ	Φ	Ψ	Φ	Ψ	Φ	Ψ	Φ	Ψ
PulA G680	ligand-free_chain_A	-81.1	100.2	-95.9	38.0	-65.8	149.6	-56.2	174.7	-107.4	-1.6
	ligand-free_chain_B	-80.0	101.0	-98.8	38.5	-71.2	159.4	-60.5	132.1	-106.5	-3.8
	G3	-80.1	103.7	-98.0	36.5	-68.4	156.4	-57.5	133.6	-111.5	-0.8
PulA-L680	ligand-free_chain_A	-82.3	105.7	-109.8	46.3	-68.3	170.3	-74.8	121.5	-108.7	170.4
	ligand-free_chain_B_Alt_A	-88.1	111.1	-82.3	42.2	113.2	159.2	-2.0	130.6	-162.2	172.6
	ligand-free_chain_B_Alt_B	-158.9	106.3	138.9	-27.0	57.5	160.0	-85.5	67.7	-116.1	44.8
	G3	-82.0	101.0	-107.1	47.5	-66.2	169.4	-72.8	124.8	-116.0	165.0
KPP	ligand-free	-145.4	168.0	169.1	-88.9	71.2	9.8	-124.7	-0.7	-65.1	133.8
	G3	-79.1	109.4	-105.9	48.6	-76.8	-165.7	-97.3	118.1	-91.8	-5.6

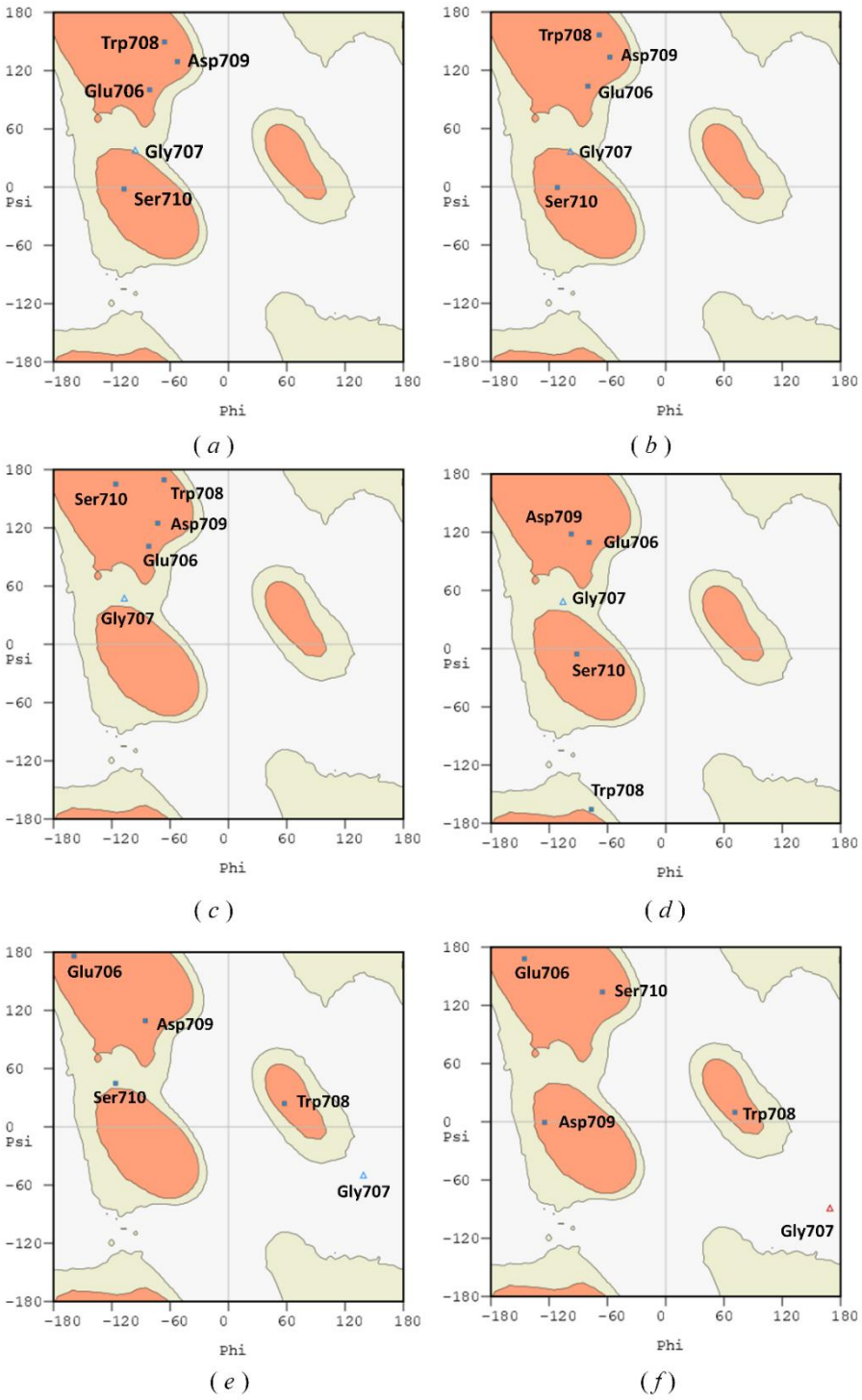

Figure 4 Ramachandran plot diagrams of residues 706-710 included loop of chain A in ligand-free PulA-G680 (*a*), in G3-complex PulA-G680 (*b*), in G3-complex PulA-L680 (*c*), in G3-complex KPP (*d*), Alt. B of chain B in ligand-free PulA-L680 (*e*) and in ligand-free KPP (*f*), respectively. These diagrams were calculated using COOT program (Emsley & Cowtan, 2004).

Table 5. The table of the interaction of between loop 706-710 and residue 680. Hydrogen bond, C-C clash contacts and C-C contacts were in the range of 2.5 Å to 3.2 Å, 3.2 Å to 4.0 Å and 4.0 Å to 4.4 Å, respectively.

		PulA-G680			PulA-L680				KPP	
		ligand-free		G3	ligand-free			G3	ligand-free	G3
Residues	Residue	A	B		A	B	B			
706-710	680					Alt. A	Alt. B			
					Hydrogen bond (Å)					
E706										
O	N	3.3	3.4	3.2	3.3	3.4	4.6	3.1	4.3	3.1
S710										
OG	O	2.7	2.6	2.6	2.9	3.2	6.9	3.4	2.9	2.7
					C-C clash and C-C contacts (Å)					
E706										
C	CD1					4.4				
C	CD2					4.2	4.2			4.4
G707										
CA	CB				4.4			4.4		4.3
C	CB				4.3	4.3		4.3		4.1
CA	CD2					3.4	3.4			
C	CD2					3.2	3.2		3.7	
C	CD1								3.6	
C	CG								4.3	
CA	CG								4.2	
CA	CD1								4.0	
W708										
CA	CD1				3.8			3.9		3.6
C	CB				4.0	4.0		4.1		3.8
C	CG				4.4	4.4	4.0			4.1
C	CD1				3.5			3.5	3.3	
CB	CD1				3.4			3.7		3.4
CG	CD1				3.9	4.4		4.3		4.2
CD1	CD1				3.7	3.7		4.2		4.3
CD1	CD2				4.4			4.4		
C	CD2					4.0	3.8			
CA	CB						4.4			4.4
CA	CG						3.9			
CA	CD2						3.3			
CD2	CD2						4.4			
CE3	CD2						3.8			
CZ3	CD2						4.4			
CE3	CD1								4.2	
D709										
C	CD1				4.0		4.1	3.8	3.8	3.3
C	CD2					3.8	4.3			
CA	CG						4.2			
C	CG						3.6			4.4
CA	CD1								3.9	3.9
S710										
CB	CA	4.1	4.1	4.1					4.3	4.4
CB	C	3.4	3.4	3.4	4.1	4.4		4.3	3.6	3.5
CA	CD1				4.0			3.9	3.7	3.6
CB	CB				3.7	3.8		3.8	3.6	3.8
CB	CG				3.5	3.5		3.6		3.4
CB	CD1				3.5			3.4	3.3	3.7
CA	CD2					3.3				
CA	CG								3.8	4.0
CB	CD2								3.9	

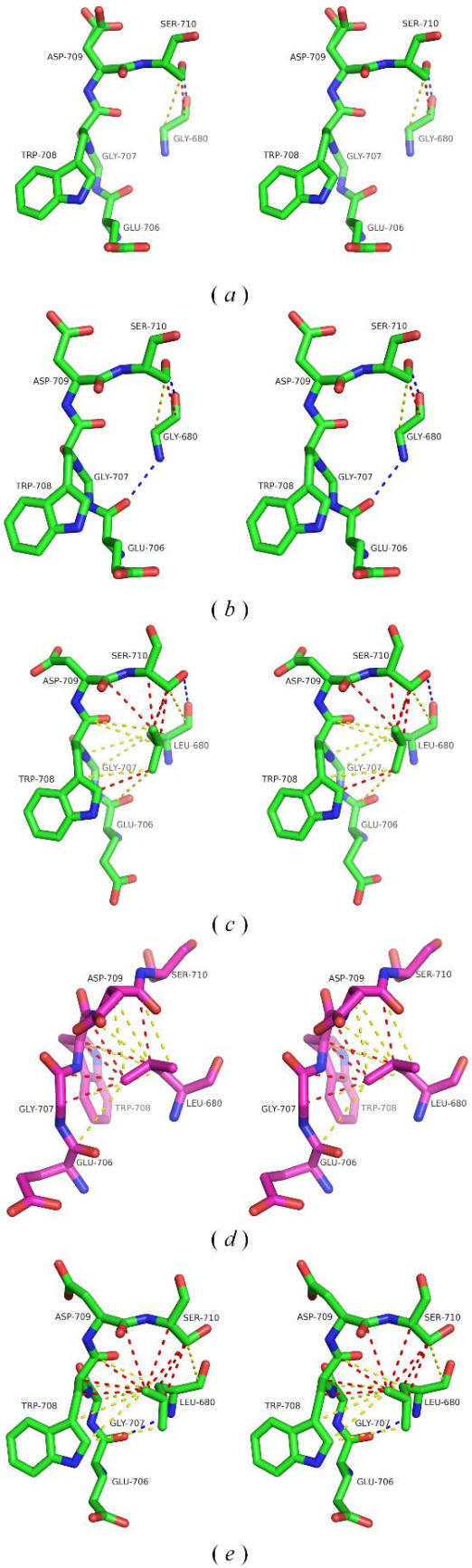

Figure 5 Stereo representations of interaction between residue 680 and 706-710 loop of chain A in ligand-free structure of PulA-G680 (*a*), in G3-complex structure of PulA-G680 (*b*), Alt. A (*c*) and B (*d*) of chain B in ligand-free structure of PulA-L680, in G3-complex structure of PulA-L680 (*e*), respectively. Green and magenta sticks show the residue of 680 and loop 706-710. Blue, red and yellow break lines show hydrogen bond (the range of 2.5Å to 3.2 Å), C-C clash contacts (the range of 3.2 Å to 4.0 Å) and C-C contacts (the range of 4.0 Å to 4.4 Å), respectively.

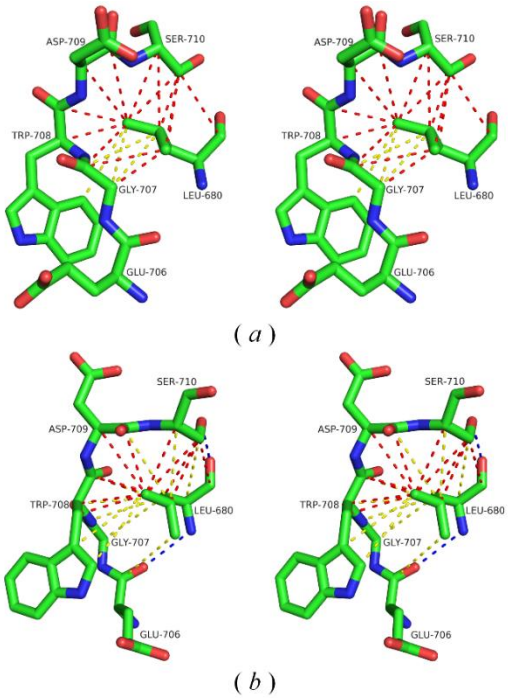

Figure 6 Stereo representations of interaction between residue 680 and 706-710 loop of ligand-free (*a*) and G3-complex structure (*b*) of KPP, respectively. Green sticks show the residue of 680 and loop 706-710. Blue, red and yellow break lines show hydrogen bond (the range of 2.5Å to 3.2 Å), C-C clash contacts (the range of 3.2 Å to 4.0 Å) and C-C contacts (the range of 4.0 Å to 4.4 Å), respectively.

4. Conclusion

In this paper, we tried to elucidate the mechanism of induced-fit motion of the active site (residues 706-710) observed in KPP by the structural and functional analysis of PulA-G680 and mutant PulA-L680 from *Klebsiella pneumoniae* ATCC 9621. Results of activity measurements of PulA-G680 and PulA-L680 indicate the decreased k_{cat} and increased K_m of PulA-L680 against pullulan. Moreover, structural analysis showed that the loop conformation of ligand-free PulA-G680, PulA-G680/G3 and PulA-L680/G3 is almost the same but the loop conformation of the ligand-free PulA-L680 (Alt. B in chain B) was different from the others as it took a similar conformation observed in the structure of ligand-free KPP (Mikami et al., 2006).

Investigation of the interaction between the side-chain of residues 680 and the mobile loop residues (706-710) suggested there were many clash distances caused by the side-chain of Leu680. These results reveal that side-chain of Leu680 involve in the change of the loop conformation and in the decreased activity. We think that decline of interaction of Trp708 with substrate by movement of the loop causes the decreased activities of KPP and PulA-L680. As shown in the ligand-free structure of PulA-L680, the side chain of Trp708 gets out of subsite +2 which was found in the structure of ligand-free KPP (Mikami et al., 2006, PDB code; 2FGZ). This Trp is important for activity of KPP as shown in previous study (Amemura et al., 1975). The side chain of Trp has potentially hydrophobicity. Therefore, it is estimated that the side chain of Trp708 in Alt. A of chain B in ligand-free PulA-L680 and ligand-free KPP are buried inside of molecule in order to increase in entropy energy. When substrate enter into the active site, the side chain of Trp708 comes out in subsite +2 because of the strong interaction between the side chain of Trp708 and glucose residue of subsite +2. The side chain of Trp708 is also important for the interaction with cyclodextrin (CD), known as pullulanase inhibitor. Conformational change of the active loop is also reported in KPP-CD complexes (Saka et al., 2018). It was reported that the K_i values of CDs against PulA-G680 are about five-times lower than that against KPP (Saka et al., 2018). Though we reported that Phe746 affects the inhibition

of KPP towards CDs, the different interactions of CDs between KPP and PulA-G680 may be explained by the conformational change of this loop between ligand-free and the complex with CDs.

References

Adams, P. D., Grosse-Kunstleve, R. W., Hung, L.-W., Ioerger, T. R., McCoy, A. J., Moriarty, N. W., Read, R. J., Sacchettini, J. C., Sauter, N. K. & Terwilliger, T. C. (2002). *Acta Cryst. D* **58**, 1948-1954. PHENIX: building new software for automated crystallographic structure determination

Amemura, A., Kitagawa, H. and Harada, T. (1975). *J. Biochem.* 77. 575-578. Role of the Tryptophan Group in the Action of Pullulanase of *Aerobacter aerogenes*

Bertoldo, C. and Antranikian, G. (2002). *Curr Opin Chem Biol.* **6**, 151-160. Starch-hydrolyzing enzymes from thermophilic archaea and bacteria

Collaborative Computational Project, Number 4. (1994). *Acta Cryst. D* **50**, 760-763. The CCP4 suite: programs for protein crystallography

Cremer, D. & Pople, J.A. (1975). *J. Am. Chem. Soc.* **97**, 1354-1358. A General Definition of Ring Puckering Coordinates

DeLano, W.L. (2002). The PyMOL molecular graphics system. DeLano scientific, San Carlos, CA.

Domań-Pytka, M. and Bardowski, J. (2004). *Crit Rev Microbiol.* **30**, 107-121. Pullulan degrading enzymes of bacterial origin

Emsley, P. & Cowtan, K. (2004). *Acta Cryst. D* **60**, 2126-2132. Coot: model-building tools for molecular graphics

Hii, S. L., Tan, J. S., Ling, T. C. and Ariff, A. B. (2012). *Enzyme Res.* Review Article, Pullulanase: Role in Starch Hydrolysis and Potential Industrial Applications

Imberty, A., Chanzy., H. and Pérez, S. (1988). *J. Mol. Biol.* **201**, 365-378. The Double-helical Nature of Crystalline Part of A-Starch

Janeček, Š. (2002). *Biologia Bratislava* 57, 29-41. How many conserved sequence regions are there in the α-amylase family?

Kuriki, T. and Imanaka, T. (1999). **87**. 557-565. The concept of the α-amylase family: structural similarity and common catalytic mechanism

Lombard, V., Golaconda Ramulu, H., Drula, E., Coutinho, P. M. & Henrissat, B. (2014). *Nucleic Acids Res*. **42**, D490-D495.

Mikami, B., Iwamoto, H., Malle, D., Yoon, H. J., Demirkan-Sarikaya, E., Mezaki, Y. and Katsuya, Y. (2006). *J. Mol. Biol.* **359**, 690-707. Crystal Structure of Pullulanase: Evidence for Parallel Binding of Oligosaccharides in the Active Site

Møller, M. S., Windahl, M. S., Sim, L., Bøjstrup, M., Hachem, M. A., Hindsgaul, O., Palcic, M., Svensson, B. and Henriksen, A. (2015). *J. Mol. Biol.* **427**. 1263-1277. Oligosaccharide and Substrate Binding in the Starch Debranching Enzyme Barley Limit Dextrinase

Murshudov, G. N., Skubak, P., Lebedev, A. A., Pannu, N. S., Steiner, R. A., Nicholls, R. A., Winn, M. D., Long, F. & Vagin, A. A. (2011). *Acta Cryst. D* **67**, 355-367. REFMAC5 for the refinement of macromolecular crystal structures

Murshudov, G. N., Vagin, A. A. & Dodson, E. J. (1997). *Acta Cryst. D* **53**, 240-255. Refinement of macromolecular structures by maximum-likelihood method

Otwinowski, Z. & Minor, W. (1997). *Methods Enzymol.* **276**, 307-326. Processing of X-ray diffraction data collected in oscillation mode

Saka, N., Iwamoto, H., Malle, D., Takahashi, N., Mizutani, K. and Mikami, B. (2018). *Acta Cryst. D* **74**, 1115-1123.

Stam, M. R., Danchin, E. G., Rancurel, C., Coutinho, P. M. and Henrissat, B. (2006). *Protein Eng Des Sel.* **19**. 555-562. Dividing the large glycoside hydrolase family 13 into subfamilies: towards improved functional annotations of α-amylase-related proteins

Svensson, B. (1994). *Plant Mol Biol.* **25**. 141-157. Protein engineering in the α-amylase family: catalytic mechanism, substrate specificity, and stability

Vagin, A. & Teplyakov, A. (1997). *J. Appl. Cryst.* **30**, 1022-1025. Molecular replacement with MOLREP

Vester-Christensen, M. B., Hachem, M. A., Svensson, B. And Henriksen, A. (2010). *J. Mol. Biol.* **403**. 739-750. Crystal Structure of an Essential Enzyme in Seed Starch Degradation: Barley Limit Dextrinase in Complex with Cyclodextrins

Yamashita, M., Matsumoto, Dai. And Murooka, Y. (1997). *J. Ferment Bioeng* **84**. 283-290. Amino Acid Residues Specific for the Catalytic Action towards α-1,6-Glucosidic Linkages in *Klebsiella Pullulanase*

Summary

1. The author revealed the crystal structures of KPP/CD complex at 1.96-2.59 Å resolution. In the complex structures with 1 mM α- and γ-CDs, one molecule of CD was found only at carbohydrate-binding module (CBM) 41. In the complex structures with 1 mM β-CD or with 10 mM α- and γ-CDs, two molecules of CDs were found both at CBM41 and the active site cleft, where the hydrophobic residue of Phe746 occupies the inside cavity of the CD rings. In contrast to the α- and γ-CDs, one β-CD was found only at the active site in the presence of 0.1 mM β-CD. These results were coincident with the solution experiments, which showed that β-CD inhibits this enzyme more than a thousand times more potently than α- and γ-CDs. The strong inhibition of β-CD is caused by the optimized interaction between β-CD and the side chain of Phe746. The increased K_i values of the F746A mutant for β-CD supported the importance of Phe746 in the strong interaction of pullulanase with β-CD.

2. *Klebsiella pneumoniae* pullulanase (KPP) belonging to glycoside hydrolase family 13 subfamily 13 (GH13_13) is an only pullulanase that was reported to perform induced-fit motion of a loop (residue 706-710) including catalytic acid/base residue of Glu706 in the active site upon binding of substrate analog based on X-ray crystal structural analysis. Comparison of pullulanase structures indicated that only KPP has Leu680 existing behind the loop, in contrast to Gly conserved in other GH13_13. The structure and activity analysis of pullulanase from *Klebsiella pneumoniae* ATCC 9621 (PulA-G680) and its mutant (PulA-L680) indicated that

the side chain of residue 680 is important for the motion of the loop 706-710 and altered binding affinity of substrate.

Acknowledgements

The author would like to express his deepest appreciation to Dr. Bunzo Mikami, Professor of Graduate School of Agriculture, Kyoto University, for his elaborated guidance, meaningful suggestion, and considerable encouragement that make his research great achievement.

The author would like to express his deeply appreciation to Dr. Hiroyuki Iwamoto, Professor of Faculty of Life Science and Biotechnology, Fukuyama University, for his constructive advice and providing sample of plasmid included *Klebsiella pneumoniae* pullulanase (PulA).

The author is deeply grateful to Dr. Kimihiko Mizutani and Dr. Nobuyuki Takahashi, Assistant Professor of Graduate School of Agriculture, Kyoto University, for his constructive advice and warm guidance.

The author deeply acknowledges Dr. Tetsuya Masuda, Assistant Professor of Graduate School of Agriculture, Kyoto University, for his thoughtful instruction about X-ray crystallography and data collection.

The author would like to acknowledge the members of the Laboratory of Applied Structural Biology, Division of Applied Life Science, Graduate School of Agriculture, Kyoto University, for their assistance.

Finally, the author would like to express special thanks to his family and friends for their best sympathetic support.

Naoki SAKA

List of Publication

1. Naoki Saka, Hiroyuki Iwamoto, Dominggus Malle, Nobuyuki Takahashi, Kimihiko Mizutani and Bunzo Mikami

   Elucidation of the mechanism of interaction between *Klebsiella pneumoniae* pullulanase and cyclodextrin.

   Acta. Crystallogr. Sect. D Struct. Biol. **74**, 1115-1123 (2018)

2. Naoki Saka, Hiroyuki Iwamoto, Nobuyuki Takahashi, Kimihiko Mizutani and Bunzo Mikami

   Relationship between induced-fit loop and activity of *Klebsiella pneumoniae* pullulanase.

   Acta. Crystallogr. Sect. D Struct. Biol. (In preparation)

Other paper

1. Taisuke Nomura, Hisamu Iwase, Naoki Saka, Nobuyuki Takahashi, Bunzo Mikami and Kimihiko Mizutani

   High-resolution crystal structures of the glycoside hydrolase family 45 endoglucanase EG27II from the snail *Ampullaria crossean*.

   Acta. Crystallogr. Sect. D Struct. Biol. (submitted)

2. Teisuke Takita, Kota Nakatani, Yuta Katano, Manami Suzuki, Kenji Kojima, Naoki, Saka, Bunzo Mikami, Rei Yatsunami, Satoshi Nakamura and Kiyoshi Yashukawa

   Increase in the thermostability of GH11 xylanase XynJ from *Bacillus* sp. strain 41M-1 using a site saturation mutagenesis library.

   J. Biochem. (submitted)

3. Wan Hasnidah Wan Osman, Bunzo Mikami, Naoki Saka, Keiko Kondo, Takashi Nagata and Masato Katahira

   Structure of a serine-type glutathione S-transferase of *Ceriporiopsis subvermispora* and identification of the enzymatically important non-canonical residues by functional mutagenesis.

   Biochem. Biophys. Res. Commun. (submitted)